ACS APPLIED MATERIALS & INTERFACES

www.acsami.org

Research Article

Fully Integrated 3D Microelectrode Arrays with Polydopamine-Mediated Silicon Dioxide Insulation for Electrophysiological Interrogation of a Novel 3D Human, Neural Microphysiological Construct

Charles M. Didier,[#] David Fox,[#] Kevin J. Pollard,[#] Aliyah Baksh, Nisha R. Iyer, Alexander Bosak, Yuen Yee Li Sip, Julia F. Orrico, Avra Kundu, Randolph S. Ashton, Lei Zhai, Michael J. Moore, and Swaminathan Rajaraman*

Cite This: *ACS Appl. Mater. Interfaces* 2023, 15, 37157−37173

Read Online

ACCESS | Metrics & More | Article Recommendations | Supporting Information

ABSTRACT: Advances within in vitro biological system complexity have enabled new possibilities for the "Organs-on-a-Chip" field. Microphysiological systems (MPS) as such incorporate sophisticated biological constructs with custom biological sensors. For microelectromechanical systems (MEMS) sensors, the dielectric layer is critical for device performance, where silicon dioxide (SiO_2) represents an excellent candidate due to its biocompatibility and wide utility in MEMS devices. Yet, high temperatures traditionally preclude SiO_2 from incorporation in polymer-based BioMEMS. Electron-beam deposition of SiO_2 may provide a low-temperature, dielectric serving as a nanoporous MPS growth substrate. Herein, we enable improved adherence of nanoporous SiO_2 to polycarbonate (PC) and 316L stainless steel (SS) via polydopamine (PDA)-mediated chemistry. The resulting stability of the combinatorial PDA−SiO_2 film was interrogated, along with the nature of the intrafilm interactions. A custom polymer−metal three-dimensional (3D) microelectrode array (3D MEA) is then reported utilizing PDA−SiO_2 insulation, for definition of novel dorsal root ganglion (DRG)/nociceptor and dorsal horn (DH) 3D neural constructs in excess of 6 months for the first time. Spontaneous/evoked compound action potentials (CAPs) are successfully reported. Finally, inhibitory drugs treatments showcase pharmacological responsiveness of the reported multipart biological activity. These results represent the initiation of a novel 3D MEA-integrated, 3D neural MPS for the long-term electrophysiological study.

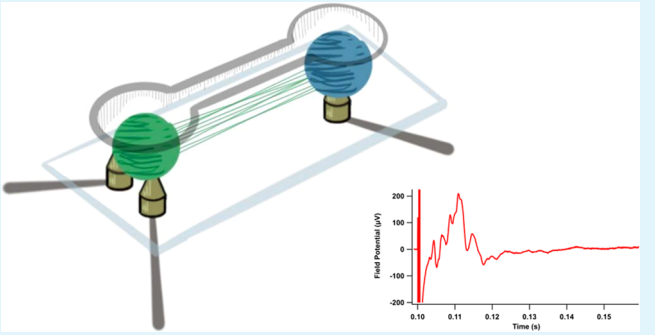

KEYWORDS: *3D microelectrode arrays (3D MEAs), silicon dioxide (SiO_2), polydopamine (PDA), neural microphysiological systems (MPS), compound action potentials (CAPs)*

1. INTRODUCTION

In recent decades, the complexity of *in vitro* biological systems has increased dramatically through the development of "Organ-on-a-Chip" models, which replicate specific organ- or tissue-level systems through benchtop data collection. Similarly, microphysiological systems (MPS) aim to incorporate highly specific cellular models that replicate precise biological functions in a benchtop form factor with integrated sensing modalities.[1−11] Importantly, the emphasis of MPS modeling *in vitro* is motivated by several factors. First, physiologically representative laboratory models could equate to more robust preclinical data for human trials (e.g., drug candidate screening and mechanism of action data). With continued development, these models could also improve patient safety by providing a route for personalized medicine.[6] After validation, the use of such *in vitro* MPS could also lead to a reduction in the usage of animal models.[6] Neural MPS are an especially attractive target for improved therapeutic drug discovery and testing as drugs targeting neurological disorders face the highest rate of attrition throughout clinical trials.[12] Due to its central role in lower afferent pain signaling, the peripheral to central nervous system junction is a crucial target for MPS development as the field works to combat the ongoing Opioid Crisis in the United States.[1,2,13,14]

Received: April 22, 2023
Accepted: June 19, 2023
Published: July 26, 2023

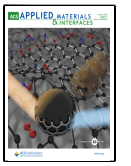

https://doi.org/10.1021/acsami.3c05788
ACS Appl. Mater. Interfaces 2023, 15, 37157−37173

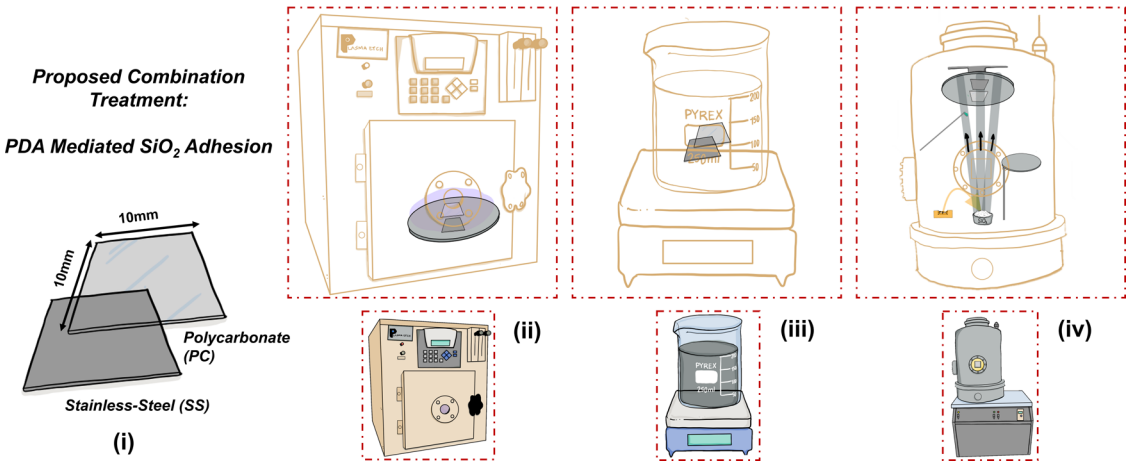

Figure 1. Schematic illustration of the proposed combination treatment for the PDA-mediated adhesion of SiO_2 to PC and SS. (i) Illustration of the 10 mm^2 PC and SS test chips. (ii) Plasma treatment chamber for the preparation of substrates prior to PDA treatment and SiO_2 deposition. (iii) Stirring solution of PDA + EDC for coating of substrates. (iv) Electron-beam deposition chamber for the sublimation of SiO_2.

Although these MPS are poised to propel the field of *in vitro* diagnostics forward,[2] innovations in the constituent device materials and tools integrated into *in vitro* tissues are required to enable the measurement of necessary functional metrics.[15−18] Identification of appropriate data collection methodologies for the model of interest, as well as material implications on both biosensor functionality and biological integration, should be treated with equal importance.[19,20] Microelectrode arrays (MEAs) have advanced greatly in recent decades, owing to sophisticated microelectromechanical systems (MEMS) processing technologies that have been established over the last several decades.[21−25] MEAs offer the distinct advantage of enabling higher throughput and automated electrophysiology compared to manual, highly serial, hand-placed recordings.[22,25] Three-dimensional (3D) MEAs as such have been established as necessary tools for interfacing with the growing complexity of *in vitro* 3D biological systems.[23,24] Within the sphere of their fabrication, polymers are becoming the preferred substrates for 3D MEA microfabrication as they are both largely biocompatible and highly tunable through microfabrication processes.[26−28] Nonreactive alloys such as stainless steel (SS) can provide the conductive bulk surfaces for microelectrode construction. However, new process integration challenges naturally arise with alternate materials. For example, insulating dielectrics are a key component of the MEA device, but traditional dielectrics may be incompatible with newer materials, preventing many potential applications.[29] Additionally, novel dielectrics that enable enhanced cellular adherence and tissue growth are necessary for integration of 3D MEAs into neural MPS.[30−32]

Silicon dioxide (SiO_2) as a dielectric material has been widely studied and utilized in traditional MEMS fabrication.[32,33] Its stability and biocompatibility have continually motivated the utilization of SiO_2 as the functional surface for many BioMEMS devices.[28,34] Alternative polymer insulation strategies are additionally well-established, including Parylene-C, and are suitable for integration with a variety of materials such as glass, polymers, composites, and conducting polymers.[35−37] Parylene-C is naturally a common choice due to its biocompatibility and transparency and can be leveraged with thin conductive materials such as such as PEDOT:PSS (poly(3,4-ethylene dioxythiophene polystyrene sulfonate)), and ITO (indium tin oxide), respectively, to produce near-transparent MEAs.[36] Parylene-C can also provide downstream processibility through protection from photoresist etchants to aid in MEA architecture definition.[35,37]

Parylene-C and SiO_2 have both been utilized as insulation materials in MEAs for their integrative properties with key proteins such as fibronectin and albumin.[38] Researchers have additionally hybridized both materials to enhance neuronal adhesion and growth.[39,40] Where the novelty and advantages of a nanoporous SiO_2-based insulation layer lies is in the architecture generated from an unannealed sublimation of the material, presenting potential benefits toward neural MPS integration.[41] Yet, challenges remain to its adaptation to nontraditional substrates and MPS integration, including 3D MEAs fabricated using polymers, metal alloys, and neural MPS. In general, SiO_2 has been deposited through thermal growth, plasma-enhanced deposition processes (such as plasma-enhanced chemical vapor deposition; PECVD), or precursor-mediated synthesis, utilizing temperatures and general process conditions hostile to polymers.[42] At such temperatures (typically between 200 and 300 °C during PECVD and much higher localized plasma temperatures), finished surfaces for common biologically relevant polymers, including polycarbonate (PC), polystyrene (PS), and poly(ethylene terephthalate glycol) (PETG), may be rendered brittle and broken.[43] Additionally, mismatch in functional groups leads to weak adhesion between SiO_2-coatings and substrates that is potentially disrupted by humidity/hydration-induced swelling.[44] Thus, alternative strategies are necessary to enhance the adhesion of SiO_2 to substrates by utilizing established intermediary compounds. Ideally, the said strategies should result in substrates with desired optical properties as well as suitable biocompatibility and should be scalable for 3D MEA microfabrication processes.

Solution-based polydopamine (PDA) treatments[45] have been previously utilized to provide a linker for such disparate materials. It is known that PDA is able to natively bind both organic and inorganic surfaces through catechol groups.[46] The specific mechanism may vary across materials and thus should be investigated to determine the suitability for a given application, including surface modifications for biological applications.[47] Owing to the rare utilization of unannealed SiO_2, we hypothesize that PDA treatment along with electron-beam sublimation of SiO_2 may provide a novel, low-

https://doi.org/10.1021/acsami.3c05788
ACS Appl. Mater. Interfaces 2023, 15, 37157−37173

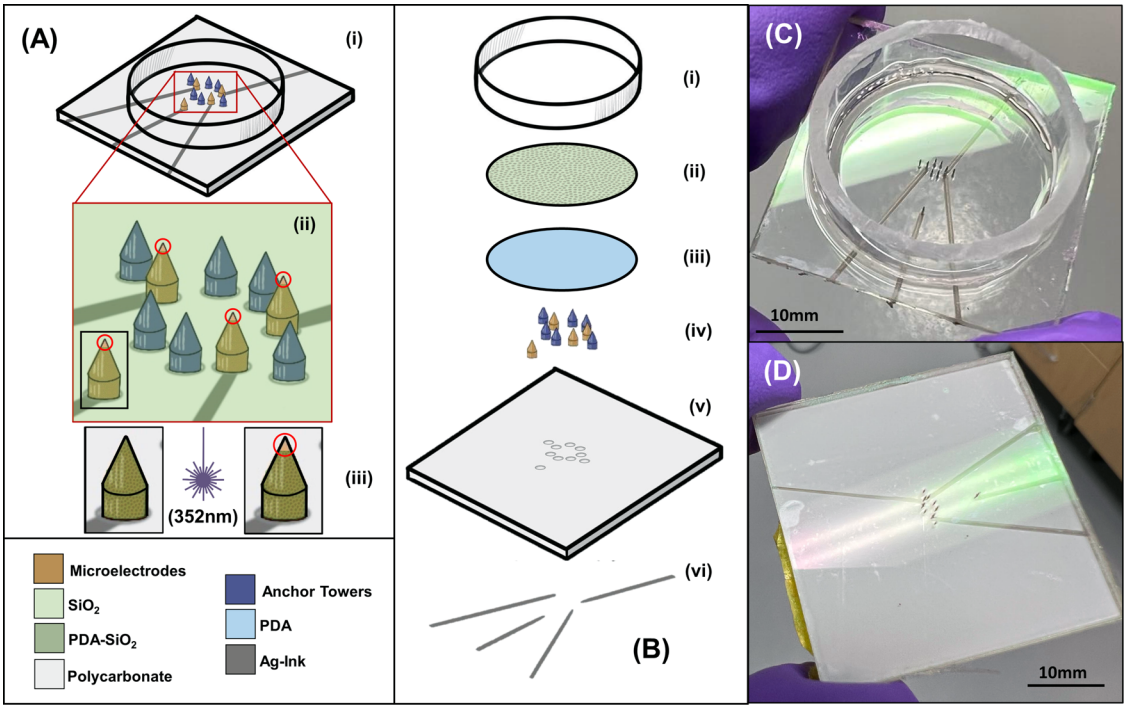

Figure 2. Schematic representation and optical images of the proposed PC and SS 3D MEA platform. (A) Assembled 3D MEA platform. (i) Schematic of the 3D MEA prior to PDA−SiO_2 insulation. (ii) Enlarged inset of the central culture region where SS microelectrode (gold) and PEG gel anchor (blue) towers are present, and additionally illustrates a conformal PDA−SiO_2 layer. Each circle denotes the proposed microelectrode recording site. (iii) Enhanced view of a singular microelectrode tower from (ii). After PDA−SiO_2 definition, precision UV−laser micromachining defines the final microelectrode recording site. (B) Expanded schematic view of the 3D MEA, separating each component layer: (i) PC culture well, (ii) nanotextured SiO_2, (iii) PDA, (iv) microelectrodes and anchor towers, (v) PC substrate with drilled vias, and (vi) Ag-ink traces. (CD) Optical images of the final 3D MEA utilized in electrophysiological studies. The green coloration (C) is additionally indicative of the desired 500 nm SiO_2 and demonstrates the more familiar purple coloration as well with a simple difference in the incidence of light (D).

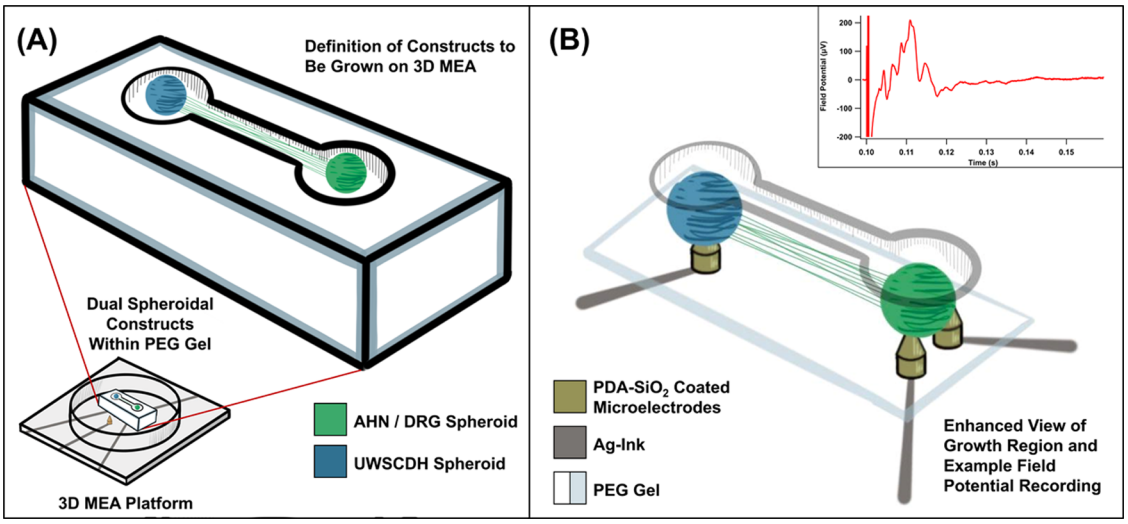

Figure 3. Schematic representation of the neural coculture definition on the 3D MEA platform. (A) Representation of the PEG gel scaffold with the AHN/DRG (green) spheroids growing their axons toward the UWSCDH (blue) spheroidal population. (B) Internal view of a neural coculture within the PEG gel scaffold with respect to its orientation on the stimulating/recording 3D MEA electrodes. The inset depicts a sample field potential recording that could be obtained from the MEA.

temperature avenue for the generation of stable, bioadherent dielectric coatings that promote robust nerve tissue growth.

Approaches utilizing novel substrate/conductor/insulation strategies have formed the basis of the 3D MEA-based neural MPS collaboratively under development between the University of Central Florida, Tulane University, and the University of Wisconsin-Madison.[15,28,31,48] The collaborative effort approaches the highly custom nature of the desired 3D MEA-enabled human neural nociceptive construct through a unique and novel approach. Herein, we report the microfabrication of a custom polymer and SS-based 3D MEA platform, which incorporated a novel PDA-enhanced adhesion of SiO_2 toward procuring functional electrophysiological recordings from a custom dual-spheroidal neural coculture in

https://doi.org/10.1021/acsami.3c05788
ACS Appl. Mater. Interfaces 2023, 15, 37157−37173

excess of 6 months. Electron-beam sublimation of nanoporous SiO_2 was characterized on polycarbonate and 316L SS microelectrode materials after development of a PDA stabilization regimen (Figure 1). We subsequently characterized this method for its robustness and optical properties. Furthermore, we presented a hypothesis for the possible mechanism of stabilization between the PDA chains and SiO_2. We then integrated this SiO_2 dielectric insulation method into our PC-SS 3D MEA process flow (Figure 2) and characterized its constituent impedimetric performance. Finally, we integrated a neural MPS system atop the 3D MEA and demonstrated the long-term growth of the custom nociceptive coculture circuit on the 3D MEA and perform confirmational inhibitory drug studies, indicating the suitability of this methodology to extract complex biological information from the recorded electrophysiological waveforms (compound action potentials [CAPs]; Figure 3).

2. MATERIALS AND METHODS

2.1. Surface Coating for Testing and Application. The overall SiO_2-coating processing steps are schematically depicted in Figure 1. Material test chips (10 mm^2 to ensure size compliance with all equipment) were micromilled from bulk sheets of a 1.75-mm-thick PC (McMaster-Carr, IL) and 50-μm-thick 316L SS (Trinity Brand Industries Inc, IL), utilizing the T-Tech QCJ5 micromilling system (T-Tech, GA). A T4-end mill bit (200 μm diameter; T-Tech Inc.) was utilized at a spindle speed of 60,000 rpm, feed rate of 25 mm/s, and a depth of cut of 2 mm. The chips were subsequently cleaned through sonication in 70% isopropyl alcohol (IPA; Sigma-Aldrich, MO) and air dried.

A stirring solution of 0.05 M w/v dopamine HCl (Sigma-Aldrich, MO) was prepared as per Azim et al.[45] in deionized (DI) water. A 1:1 molar ratio solution was then prepared by utilizing a stock 0.1 M w/v 1-ethyl-3-(3-dimethylaminopropyl)-carbodiimide (EDC; Alfa Aesar, MA) solution as a polymerization enhancer, bringing the pH value of the solution to 8. Test chips were subsequently plasma-treated (PE-50; Plasma Etch Inc., NV) in ambient, mixed-air plasma (50 W power) for 1 min and then submerged in the stirring PDA solution between 1 and 3 h. After the desired 1, 2, or 3 h timepoint, the test chips were rinsed three times in DI water, dried with N_2 gas, and stored under vacuum. PDA-coated chips were again plasma-treated for 1 min prior to the electron-beam deposition of 500 nm SiO_2 (Thermionics Laboratories Inc., CA). Additional test chip treatments were prepared for analysis, control, and comparison.

2.2. 3D MEA Fabrication. *2.2.1. Substrate Definition.* The 3D MEA microfabrication process flow prior to PDA−SiO_2-coating is detailed in Figure 2. Substrates for the 3D MEA fabrication were micromilled to a size of 30 mm^2 from 1.75-mm-thick PC, utilizing T-Tech QCJ5 micromilling machine (T-Tech Inc., GA). This size was chosen to replicate similarly available commercial MEA footprints. Four traces were milled utilizing a silicon carbide, T4-end mill bit (200 μm diameter; T-Tech Inc., GA) at a spindle speed of 60,000 rpm, feed rate of 25 mm/s, and a depth of cut of 500 μm. A silicon carbide microdrill bit (0.0083″; T-Tech Inc., GA) was then inserted into the machine to drill four through-vias corresponding to the location of the microelectrode towers at the end of each trace along with six vias that would define the anchor towers around the central electrodes (spindle speed 90,000 rpm, feed rate 25 mm/s, depth of cut 2 mm). The four microelectrode vias were centrally aligned, with two placed 2 mm across from the third, and the fourth to act as a reference electrode, located centrally 10 mm from other three. The overall substrate was subsequently released from the bulk PC utilizing the same T4-end mill bit and parameters as the traces, but with a fully releasing depth of cut of 2 mm.

PC tubing (22 mm ID/25 mm OD; McMaster-Carr, IL) was cut to a height of 6 mm to define the culturing area of the device. Standard 10:1 poydimethylsiloxane (PDMS; Sylgard-184, Dow Corning, MI) was mixed and then degassed in a bell jar vacuum system for 30 min. The culture well was affixed to the topside of the substrate utilizing PDMS and allowed to cure for 1 h at 60 °C.

2.2.2. Microelectrode Tower Definition and Insertion. 250 μm diameter SS needles (Lhasa Ohm, MA) were cut to a height of 2.25 mm, utilizing a custom infrared (IR) laser-scribing approach (Quik Laze 50ST2; Eolite Lasers, OR). Ten needles per device were subsequently inserted from the backside of the device, utilizing a magnetic insertion approach,[48] to define the final height of the needles above the surface of the substrate at ∼500 μm.

2.2.3. Conductive Silver Ink-Casting. A biocompatible silver (Ag) epoxy (EP3HTSMED, MasterBond Inc., NJ) was cast across the backside of the device to fill in the micromilled traces and the remainder of the vias. The backing layer of the PC after micromilling served as the mask for casting, and 70% IPA was additionally utilized to remove excess ink. The ink-cast devices were placed in an oven and cured at 60 °C overnight. At this stage, the 3D MEAs were considered in their uninsulated state with tall (∼500 μm) microtower electrodes.

2.2.4. PDA Treatment and Oxide Definition. A stirring PDA solution was prepared as per Section 2.1, and fabricated 3D microtower MEAs were affixed inside a glass dish. Each MEA was plasma-treated for 1 min before being submerged in the PDA solution for 2 h. The MEAs were subsequently washed in DI water three times and dried with N_2 gas. The MEAs were plasma-treated once again for 1 min, and then placed into an electron-beam deposition chamber for the deposition of 500 nm SiO_2 at a deposition rate of 1−2 A/s. At this stage, the MEAs were considered to be insulated with bulk SiO_2. Lastly, the 3D MEAs were precision-deinsulated, utilizing ultraviolet (UV) laser micromachining (Quik Laze 50ST2; Eolite Lasers, OR) with a 30 μm spot size and conditions as per Kundu et al. (4 ns pulse, 532 nm wavelength, 1.2 mJ power).[28] At this stage, the microfabrication was fully complete.

2.3. Characterization. *2.3.1. Sample Imaging.* Scanning electron microscopy (SEM) was performed on the Zeiss NVision system (Zeiss, Germany) for surface comparisons, and optical images of fully completed 3D MEAs were obtained using iPhone 13 (Apple Inc., CA). For visualization of organoid growth, Calcein AM (CAM; Thermo-Fisher Scientific, MA) staining of tissue was performed utilizing the Nikon AZ100 system (Nikon, Japan). Laser confocal microscopy (Keyence VK-X3000; Keyence, Japan) was performed at 50× magnification, utilizing combination laser and confocal scanning settings. Extraction of values was performed in the VK-X3000 Analyzer Suite software (Keyence, Japan). ImageJ software (National Institutes of Health, MD) was utilized for image-based quantifications.

2.3.2. Chemical and Surface Analysis. Energy dispersive X-ray spectroscopy (EDS) was performed as confirmation of deposited SiO_2 composition during SEM imaging (Zeiss NVision; Zeiss, Germany). The elemental composition of layered SiO_2−PDA−PC samples was additionally determined through EDS using high-resolution transmission electron microscopy (HRTEM). For HRTEM preparation, a thin cross-sectional specimen of the device was prepared using a TEM focused ion beam (FIB) instrument (FEI 200; FEI Co., OR). The specimen was then studied utilizing the FEI Tecnai F30 (FEI Co., OR). High-resolution imaging was conducted in scanning transmission electron microscopy (STEM) mode with an annular dark field detector. The elemental composition and distribution across an area of the specimen were determined using EDS analysis and elemental mapping. The maps were colored to distinguish the studied elements, with the color intensity demonstrating the degree of distribution across the scanned area.

X-ray photoelectron spectroscopy (XPS; 5400 ESCA; Physical Electronics, MN) was utilized for chemical analysis and additional compositional confirmation of the PDA-coupled SiO_2 film. A layer of 10-nm-thick SiO_2 films was deposited onto 2 h PDA-coated samples for XPS scans.

To assess the relative adhesion of deposited SiO_2 films to PC and SS substrates, a standard tape peel test was employed,[49] however, utilizing a manual application and removal method. Scotch tape was applied to substrates with a nominal 10 Pa force and then removed at a rate of 1 mm/s with the tape peeled at ∼90° with respect to the surface. To simulate MEA dielectric layer stability in cell culture

https://doi.org/10.1021/acsami.3c05788
ACS Appl. Mater. Interfaces 2023, 15, 37157−37173

incubator conditions, SiO_2−PDA-coated SS chips were subjected to an incubator environment (>95% humidity) at 4, 6, and 10 week time periods, before scotch-tape peel-test analysis of the adhesion was performed.

Water contact angle (WCA) measurements were obtained (Goniometer, OCA 15EC mode, SCA 20 module; DataPhysics Instruments GmbH, Germany) to assess the relative surface energies across functionalization states. Ultraviolet−visible spectroscopy (Agilent Tech., CA) was performed to assess transparency of the PDA−SiO_2-coated PC substrates.

Atomic force microscopy (AFM; tapping mode, 13−77 N/m tip, 0.75 Hz scan rate, 1 V set point; NanoIR2, Anasys Instruments) was utilized to obtain profilometric measurements of the aqueously deposited PDA film on test substrates.

2.3.3. Impedimetric Characterization. Impedance spectroscopy was performed utilizing the BODE 100 impedance analyzer system (Omicron Labs, Austria) across the 100 Hz−40 MHz frequency spectrum. Readings were acquired in Dulbecco's phosphate-buffered saline (DPBS; Sigma-Aldrich, MO) with a platinum (Pt) counter electrode. Equivalent-circuit fittings and parameter extractions were performed utilizing the EIS Spectrum Analyzer Software (EIS Spectrum Analyzer Software, Belarus; 300 iterations, Powell algorithm, amplitude function).[50,51] A modified Randles equivalency circuit was chosen to fit the data, with a constant phase element (CPE) replacing the double layer capacitance (C_{DL}) for more flexibility in fitting.[52,53] All values reported were generated with relative errors of less than 5%.

2.4. Cell Culture. *2.4.1. Primary Rat-Derived Cultures. 2.4.1.1. Generation of 3D Spheroid Cultures.* All animal handling and tissue harvesting procedures were performed according to guidelines set by the American Veterinary Medicine Association and approved in advance by the Institutional Animal Care and Use Committee (IACUC) at Tulane University. Schematic representations of cellular growth and integration within the 3D MEA are detailed in Figure 3. Rat tissues were harvested and formed into neural spheroids as previously described.[1] Briefly, timed-pregnant Long−Evans rats were purchased from Charles River Laboratories (Wilmington, MA). Dorsal root ganglia (DRG) from an entire embryonic day 15 (E15) rat litter were harvested, pooled, and digested in 0.25% trypsin in PBS with EDTA, pH 7.4 (Thermo-Fisher Scientific, MA) for 15 min at 37 °C. The digested tissue was dissociated through trituration into a single-cell suspension and passed through a 40 μM nylon mesh filter. The cells were then seeded in 96-well ultralow attachment spheroid microplates (Corning Inc., NY) at 45,000 cells per well in rat growth media composed of Neurobasal Medium supplemented with 2% v/v B27 supplement, 1% v/v N2 supplement, 1% v/v GlutaMAX, 20 ng/mL nerve growth factor 2.5S native mouse protein, 10 ng/mL recombinant human/murine/rat brain-derived neurotrophic factor (PeproTech, NJ), 10 ng/mL recombinant human glial cell-derived neurotrophic factor (PeproTech), and 1% v/v antibiotic/antimycotic solution (all from Thermo-Fisher Scientific, MA, unless otherwise noted). Microplates were centrifuged at 500*g* for 5 min, and 3D spheroid cultures aggregate after 48 h incubation at 37 °C and 5% CO_2.

2.4.1.2. Micropatterning Microphysiological Nerve Cultures. Fabrication and validation of 3D peripheral nerve cultures has previously been described extensively.[1,30,54−58] Single spheroids were seeded at one end of dual-hydrogel culture scaffolds using digital projection lithography similar to a previously described method.[1,54] First, 3D MEAs were prepared ahead of time for culture by filling each with DPBS supplemented with a 1% v/v antibiotic/antimycotic solution (Thermo-Fisher) and exchanging this solution once per day for 7 days. Growth-restrictive outer gels were first fabricated on transwell membranes (Corning Inc., NY) by photo-crosslinking a solution of 10% w/v poly(ethylene glycol) dimethacrylate (PEG, Polysciences Inc., PA), 1.1 mM lithium phenyl-2,4,6-trimethylbenzoylphosphinate (LAP; Allevi, PA), and 0.0001% w/v TEMPO (Millipore-Sigma, MO) in phosphate-buffered saline (PBS, pH 7.4) with ultraviolet (UV) light patterned to create a long, thin inner void, with a bulb on one end for spheroid placement surrounded by a PEG mold. A single DRG spheroid was placed in the bulb at one end of each outer-gel mold with a pipette, the void was filled with a growth-permissive inner-gel solution composed of Matrigel (Corning Inc., NY) diluted 1:1 with rat growth media, and the construct was incubated for 15 min at 37 °C to cure the Matrigel. Culture media was added underneath the transwell membrane for each construct and cultures were then returned to the incubator for maturation.

2.4.1.3. Maturation of Microphysiological Nerve Cultures. Assembled dual-hydrogel DRG-spheroid cultures were incubated for 31−35 days in culture medium, changed on Monday, Wednesday, and Friday, during which time neurites extend unidirectionally from the site of spheroid placement along the growth-permissive channel. Mature constructs are comprised of a head (or ganglion) region ("DRG") located at the site of spheroid placement (location of neuronal soma) and a tail region of neurite outgrowth ("nerve") reaching up to 8 mm in length.

2.4.2. IPSC Human-Derived Cultures. 2.4.2.1. Generation of 3D Spheroid Cultures. Cryogenically preserved human stem-cell-derived spinal cord dorsal horn (SCDH) precursor cells were provided by the laboratory of Prof. Randolph Ashton at the University of Wisconsin-Madison (UWSCDH).[59] Upon receipt, the cells were rapidly thawed and diluted 1:4 in Neurobasal Medium (Thermo-Fisher Scientific, MA). The cells were centrifuged at 300*g* for 4 min and the supernatant was removed. The cells were subsequently resuspended in neuronal differentiation media comprised of Neurobasal Medium supplemented with 2% v/v B27 supplement (Thermo-Fisher), 1% v/v N2 supplement (Thermo-Fisher), 1% v/v GlutaMAX (Thermo-Fisher), 20 ng/mL human nerve growth factor, 10 ng/mL recombinant human/murine/rat brain-derived neurotrophic factor, 10 ng/mL recombinant human glial cell-derived neurotrophic factor, 10 ng/mL recombinant human NT-3 (all growth factors from PeproTech, NJ), 1 μM dibutyryl-cAMP (Millipore-Sigma, MO), 10 μM Y-27632 (Abcam, Waltham, MA), 10 μM DAPT (Tocris, MN), and 1% v/v antibiotic/antimycotic solution (Thermo-Fisher). The cells were plated at 500,000 cells/cm^2 on culture well plates coated with Matrigel (Corning) diluted at 1:100 for 6 days in neuronal differentiation media changed every other day to induce terminal neuron differentiation.

Cryogenically preserved human stem-cell-derived nociceptors were purchased from Anatomic, Inc. (AHN; MN). The cells were rapidly thawed, diluted 1:4 in Neurobasal Medium, centrifuged at 300*g* for 4 min, and the supernatant was removed. Nociceptors were then resuspended in human culture growth media (identical to neuronal differentiation media but lacking DAPT) plated at 60,000 cells/cm^2 in well plates coated with Matrigel diluted at 1:100, allowed to adhere overnight, and washed to remove any dead cell debris. Nociceptor and terminally differentiated SCDH cell cultures were lifted by incubation in AccuMax (Thermo-Fisher) at 37 °C for 15 min. The cell suspensions were collected, centrifuged at 300*g* for 4 min, the supernatant was removed, and both cell types were resuspended in culture growth media. The cells were then seeded in 96-well ultralow attachment spheroid microplates (Corning) at a concentration of 20,000 cells per well and microplates were centrifuged at 500*g* for 5 min. 3D neural spheroids were allowed to aggregate for 48 h at 37 °C and 5% CO_2.

2.4.2.2. Micropatterning Microphysiological Nerve Cocultures. Human microphysiological cocultures of nociceptor and SCDH spheroids were patterned with the same methodology as the rat-DRG cocultures, with the following exceptions: 3D MEAs were prepared for culture by filling each with DPBS supplemented with a 1% v/v antibiotic/antimycotic solution (Thermo-Fisher) and exchanging this solution once per day for 7 days. PEG gels were then patterned directly on to the washed MEAs. The framing PEG gel was patterned into a smaller construct, forming a thin channel of 2 mm length, with an 800 μm diameter bulb at each surrounding the built-in electrodes and defining the space. An AHN spheroid was placed within one such bulb, on top of the stimulating electrodes, while a UWSCDH spheroid was placed in the opposite bulb, on top of the recording electrode. The channel was then filled with Matrigel diluted 1:1 with human

https://doi.org/10.1021/acsami.3c05788
ACS Appl. Mater. Interfaces 2023, 15, 37157−37173

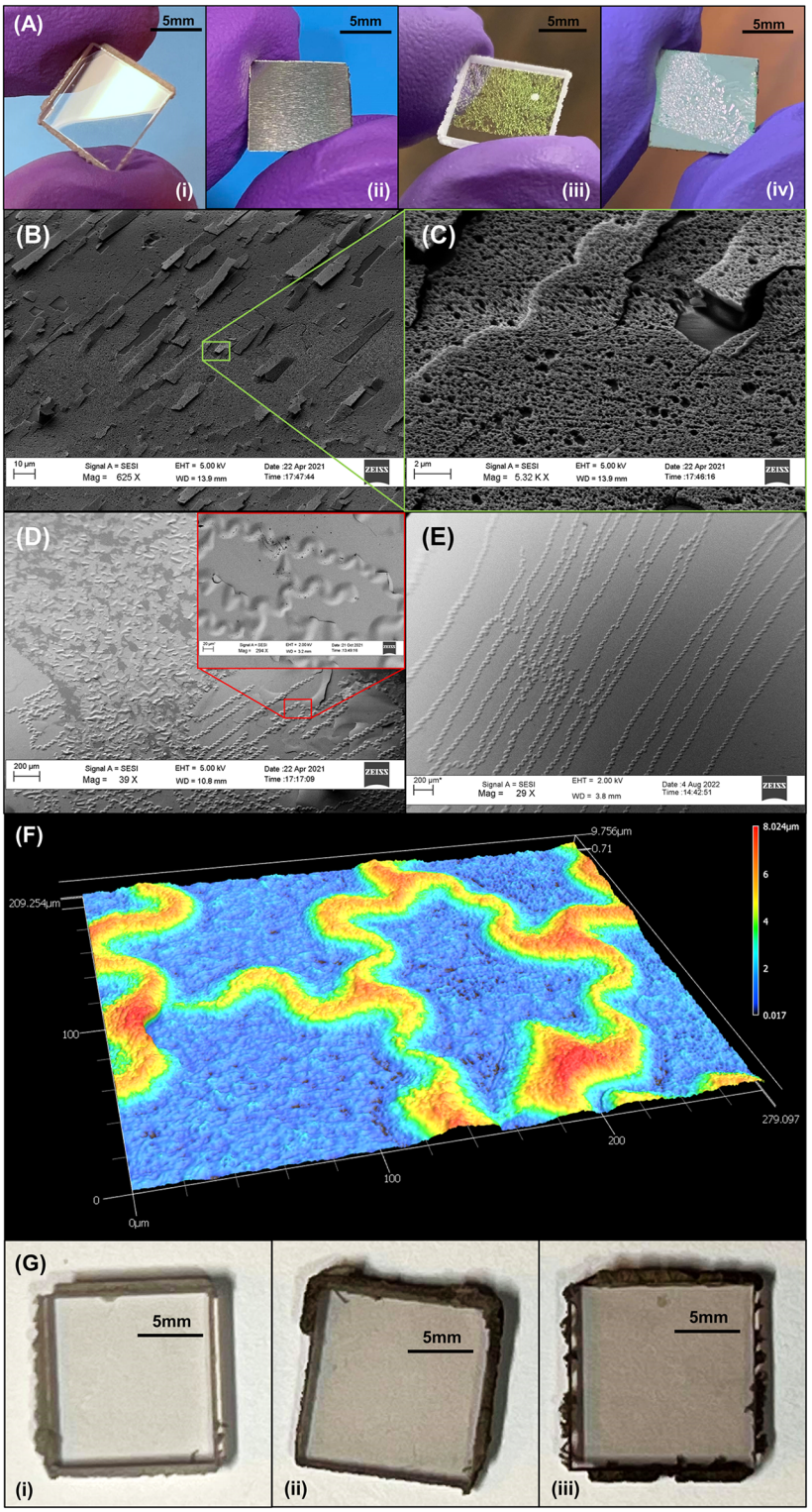

Figure 4. SEM, laser confocal, and optical imaging of the common failures in deposited 500 nm SiO_2 thin films. (A) Optical imaging of PC and SS test substrates. (i) PC test chip before treatments. (ii) SS test chip before treatments. (iii) PC test chip with 500 nm of nonadherent SiO_2. (iv) SS test chip with 500 nm of nonadherent SiO_2. (B) Cantilever-style flaking and breakage was observed in samples that had no form of pretreatment, prompting the investigation into potential mechanisms for adhesion. (C) Enhanced view of panel (B) further detailing the cracks and flaking of the oxide. Here, the porosity of the electron-beam-deposited film can be seen. (D) Imaging of samples that did not contain an optimized PDA pretreatment regimen. Buckling of the film is apparent, and the inset further details this mode of failure. (E) Isotropic buckling failure of the oxide film, which appeared to branch when surface defects were encountered under suboptimal treatment conditions, such as the lack of plasma pretreatment. (F) Laser confocal imaging of the nonadherent oxide from panels (C, D). The buckling failure mode is readily apparent, detailing the branching observed. (G) Optical images of PC chips after (i) 1 h, (ii) 2 h, and (iii) 3 h of PDA treatment.

https://doi.org/10.1021/acsami.3c05788
ACS Appl. Mater. Interfaces 2023, 15, 37157−37173

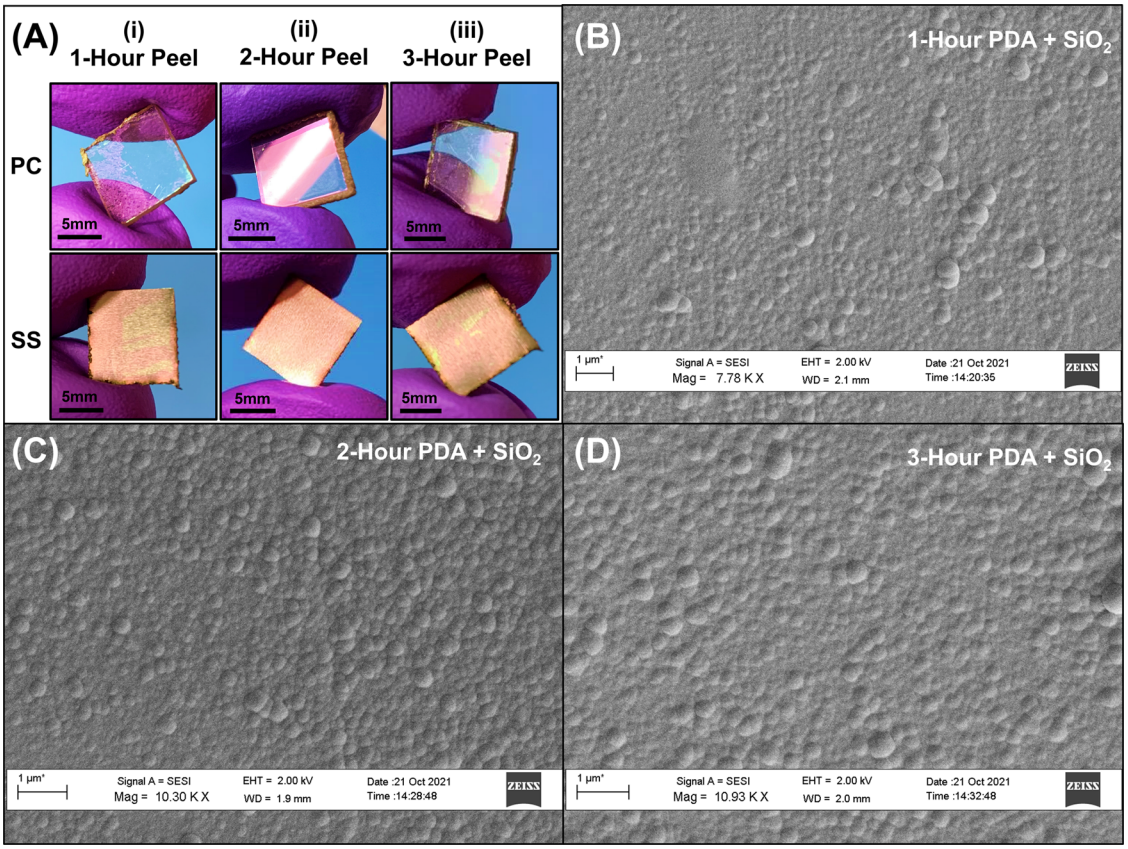

Figure 5. Optical and SEM imaging of 1−3 h PDA-coated test chips with 500 nm of SiO_2. (A) Optical images of PC and SS test chips after scotch-tape-peels. The 1 h samples (i) demonstrated partial delamination after a single peel. The 2 h samples (ii) performed the most optimal, leaving the full film intact after >20 peels. The 3 h samples (iii) were not as robust as the 2 h samples, and partially delaminated after a singular peel, however, maintained a greater integrity than the 1 h samples. (B−D) This is likely in part due to the cluster formation of the PDA−SiO_2 combination, increasing the surface roughness in a more uniform, monodisperse manner to alleviate thin-film stresses, as seen in the 2 h SEM (C).

culture growth media and was cured for 15 min at 37 °C. Cultures were then returned to the incubator for maturation.

2.4.2.3. Maturation of Microphysiological Nerve Cultures. Assembled dual-hydrogel AHN-UWSCDH cultures were incubated for 60−180 days in human culture growth medium, changed on Monday, Wednesday, and Friday, during which neurites extend from the nociceptor spheroid along the permissive growth channel to innervate the SCDH spheroid at the opposite end of the channel.

2.4.2.4. Calcein AM Viability Assay. Calcein AM (Thermo-Fisher Scientific) was used according to the manufacturer's instructions. Constructs were imaged on a Nikon AZ100 and images were processed in ImageJ.

2.5. Field Potential Recordings. Impulse conduction in all microphysiological nerve cultures was evaluated using extracellular, field potential recordings (represented by CAPs) as per previous extensive description.[1,30] All recordings were obtained utilizing a custom equipment arrangement (P-97, ALA Scientific Instruments, NY). Each evoked recording presented represents the average of 10 consecutive evoked responses (N = 10). Spontaneous recordings are not time-locked and therefore cannot be averaged. Each presented spontaneous recording is a single trace that is representative of 10 similar traces recorded under identical conditions (N = 10).

2.5.1. Rat Tissue. Mature dual-hydrogel cultures were manually transferred from transwell membranes to prefabricated 3D MEA devices with the ganglion region containing the highest density of neuronal soma laying directly atop of the microelectrode recording site. Cultures on MEAs were continuously bathed with room-temperature artificial cerebrospinal fluid (ACSF) and continuously bubbled with a gas mixture of 95% O_2 and 5% CO_2. A platinum and glass recording electrode (64-0818, Warner Instruments, CT; 1 MΩ resistance) was lowered manually into the ganglion region and a platinum stimulating electrode was placed 4−6 mm distal to the recording electrode in the middle region of neurite outgrowth. Bipolar 40 V, 200 μs stimuli were delivered once per minute to the middle of the nerve outgrowth and the resulting CAP propagation was recorded in the ganglion region by both the built-in 3D MEA microelectrode as well as through the external glass and platinum field recording electrode (N = 10).

2.5.2. Human Tissue. Dual-hydrogel human cocultures were matured directly on 3D MEAs with the SCDH region arranged directly atop the microelectrode recording site and the AHN spheroid direclty atop the microelectrode stimulation site. To record bioelectric impulses, growth media was removed and cultures were continuously bathed with room-temperature ACSF continuously bubbled with a gas mixture of 95% O_2 and 5% CO_2. When necessary, an additional platinum and glass recording electrode (1 MΩ resistance) was lowered into the SCDH spheroid region and a platinum stimulating electrode was placed in the innervating nociceptor spheroid. 40 V, 200 μs stimuli were delivered once per minute to the middle of the nociceptor spheroid by either the integrated 3D MEA stimulating microelectrode or the bipolar external field stimulating electrode. The resulting synaptically evoked waveforms were recorded in the SCDH spheroid region by a built-in 3D MEA recording microelectrode or the external glass and platinum field recording electrode, as desired (N = 10).

For confirmation of biological activity, inhibitory drugs as defined below were added to the bubbling ACSF bathing the neural cocultures, as informed by previous studies:[1]

10 μM cyanquixaline (CNQX; AMPA receptor antagonist; C239-5MG, Millipore-Sigma), dissolved in DMSO at 10 mM and diluted 1:1000 for use at 10 μM in 0.1% DMSO.

https://doi.org/10.1021/acsami.3c05788
ACS Appl. Mater. Interfaces 2023, 15, 37157−37173

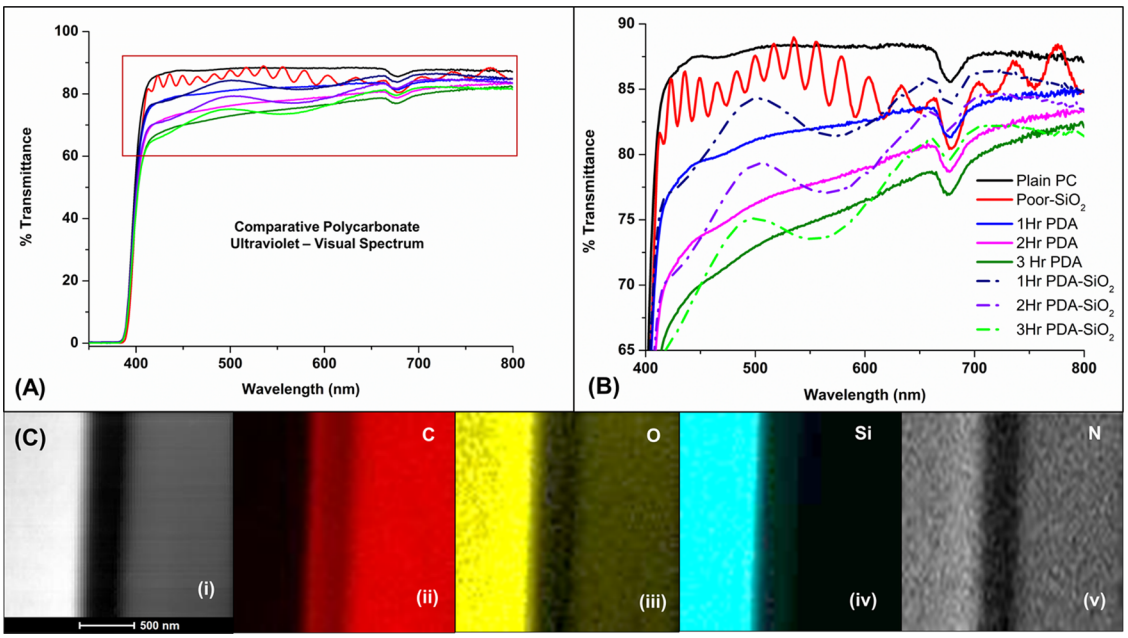

Figure 6. Film characterization measurements. (A, B) Transparency assessments of PC test chips after PDA treatments and SiO_2 deposition. (A) UV−vis spectroscopy measurements of different stages of PC test chip treatments. (B) Enhanced 400−800 nm region of interest from panel (A). A gradual loss of transparency is observed with increased PDA treatment time; however, this is partially recovered with the addition of the 500 nm SiO_2. An antireflective signature is present in all samples containing SiO_2, including the poorly adherent samples such as in Figure 4. (C) HRTEM-generated image colorations of the sample cross section utilizing the 2 h PDA treatment time. The contrast between layers can be visualized in (i). Carbon (ii) is present in the medial and PC layers as expected. Oxygen (iii) is present throughout, though dominantly in the oxide layer. Silicon (iv) is largely present in the oxide layer, but can be partially observed within the medial layer, lending credence to the notion of a bonding event with the PDA linker. Nitrogen (v) does not appear in coloration, as its relative abundance is much lower than the other elements (Figure S2).

1 μM tetrodotoxin (TTX; voltage-gated sodium channel blocker; AB120054, Abcam, U.K.), dissolved in DMSO at 1 mM and diluted 1:1000 for use at 1 μM in 0.1% DMSO.

3. RESULTS AND DISCUSSION

3.1. Characterization of PDA−SiO_2 Thin Films and Interactions. The utilization of electron-beam deposition was a direct result of experimental efforts to induce formation of an oxide coating on the polycarbonate surface via traditional deposition methods. The resulting polymer surface was not intact and thus necessitated the use of a lower-temperature deposition technique. Through e-beam technique, the maximal temperature would be located at the polymer surface, and at significantly lower temperatures (80 °C in this example), gas-phase reactions would not occur,[60] outside of more custom PECVD enclosures.[61] Smaller chip sizes when compared to the full 3D MEA footprint were utilized for higher throughput in experimentation.

In early trials of the deposited SiO_2 to PC prior to the incorporation of PDA, layers of porous and flaking SiO_2 film were observed optically and confirmed under SEM (Figure 4A−C). However, these early images confirmed the nanoporous nature of the silicon dioxide film, which indicated potential suitability for cellular applications. Previously published data by our groups and internal studies confirmed 500 nm SiO_2 films were sufficient as both a suitable dielectric and a stable insulation layer for 3D MEAs,[28] indicating that 500 nm film thickness could offset potential dielectric failure during operation with MPS. As PDA was incorporated (before treatment optimization), failure in the films was largely observed as isotropic buckling and blistering, typical failure modes for compressive strain in thin films.[62,63] In such suboptimal treatment conditions, this buckling was clearly visible under both SEM (Figure 4D,E) and laser confocal imaging and provided an optical interference pattern (Figure 4F).

Azim et al.[45] concurrently demonstrated success in adhering dissimilar polymers utilizing a solution-based PDA regimen, which indicated the potential for utilizing a PDA protocol for adhering materials to both PC and SS. It was determined based on the results contained in Azim's study that polymers would very quickly discolor with continued deposition and polymerization of the PDA (within only a few hours). To balance the need for this adhesion intermediary compound, and retention of optical clarity, deposition treatment times of 1, 2, and 3 h were tested. As shown in Figure 4G, even within a short treatment time of 3 h, noticeable darkening of the PC test chip was observed. For SS test chips, although PDA deposition was present, clarity was not of issue. As the next step, the ultraviolet−visible spectrum of different stages of coated PC substrates was tested to ensure the usability of the selected coating time/method for transmitted light biological imaging application. AFM measurements were performed to determine the time-dependent thickness of PDA-coatings. Averaged film thicknesses were measured to be 37.0, 58.3, and 83.0 nm at 1, 2, and 3 h, respectively. The mean surface roughness of each timepoint was additionally measured to be 28.3, 58.3, and 63.8 nm at 1, 2, and 3 h, respectively.

To determine the robustness of the adherence of the SiO_2 film to both the PC and SS samples, scotch-tape peel analysis was performed. After single tape-peels from PC and SS samples, it was rapidly observed that the 2 h PDA−SiO_2 samples performed as desired. Both the 1 and 3 h samples demonstrated near-total (87.4 ± 9.32%) and partial (66.2 ±

https://doi.org/10.1021/acsami.3c05788
ACS Appl. Mater. Interfaces 2023, 15, 37157−37173

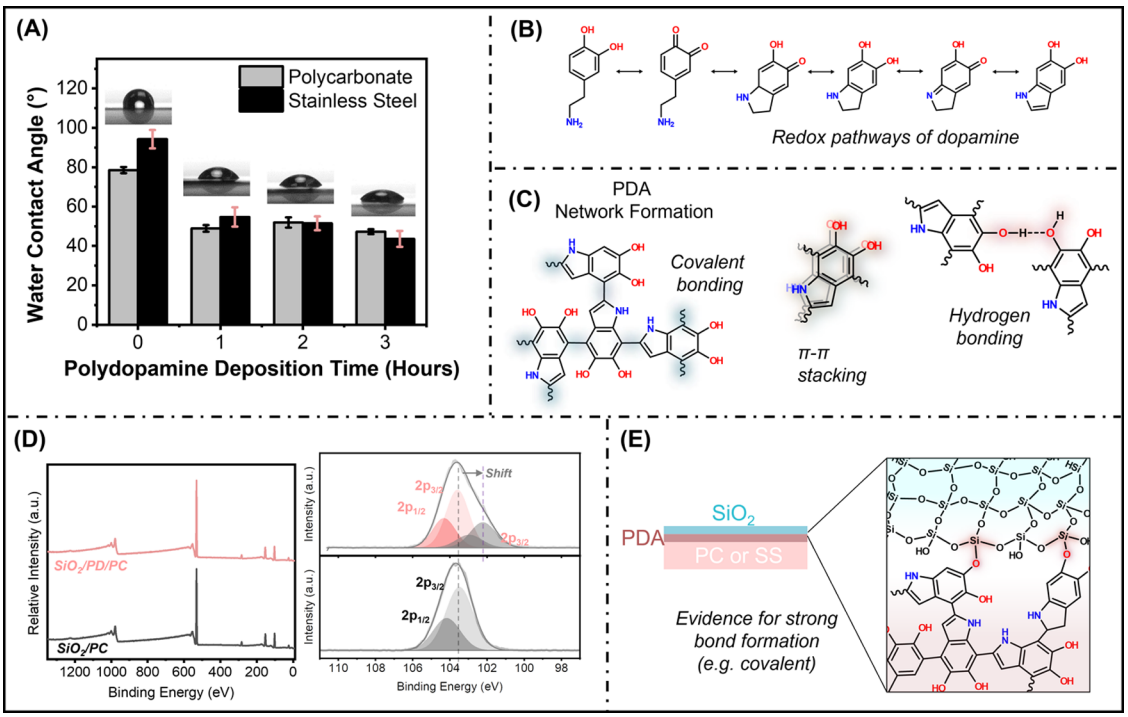

Figure 7. Chemical and surface characterization of the combinatorial PDA−SiO_2 treatment. (A) Water contact angle measurements of the SS and PC surfaces, before and after PDA film growth. (B) Representation of the various oxidation states of dopamine through 5,6-dihydroxyindole. (C) Various interactions of polydopamine, including the covalent bonding and hydrogen bonding, $\pi-\pi$ interactions. (D) XPS survey spectra and high-resolution spectra of the Si 2p electron, of the 10 nm SiO_2 on PC and PDA-coated PC. (E) Representation of potential covalent coupling to explain the improved adhesive strength and shift in XPS spectra.

15.8%) removal of the oxide film, respectively, across six peels in the areas tested. The 2 h samples retained their integrity as shown in Figure 5A. These samples additionally withstood >20 tape-peels before minor film breakage was observed around the edges of the test chips (removal of 0.63 ± 0.31%). To further motivate the usage of the 2 h PDA treatment, SS samples (to mimic the dielectric insulation on microelectrode materials) were placed into an incubator (Figure S1A). Samples were tested at 4, 6, and 10 weeks. After >20 peel tests, the 4 week samples proved highly stable, with the removal of 0.89 ± 0.935% SiO_2 (i.e., more than 99% SiO_2 was intact). After 6 weeks, 6 peel tests removed 16.5 ± 7.49% of the film. After 10 weeks, 6 peel tests removed 41.2 ± 37.3% of the film and represent the highest variability among the measurements. Importantly, only adherence of the film and not its integrity was affected, indicating that the chosen PDA−SiO_2 combination helped to alleviate the compressive stress in the film, even when long-term hydration disrupted the binding to the substrate.

With respect to the deposited PDA clusters with SiO_2, changes in both size and uniformity were observed (Figure 5B−D). Both 1 and 3 h PDA treatments coupled with deposited 500 nm SiO_2 were observed to have a more polydisperse topography to the resultant films (average cluster radii of 301 ± 147 nm and 311 ± 120 nm, respectively). This was contrasted with the 2 h PDA deposition, which demonstrated a more monodisperse layer and may have additionally aided in stabilizing the SiO_2 film (average cluster radii of 307 ± 63 nm). The resulting robustness of the 2 h PDA−SiO_2 combination provided rationale for its use in the final 3D MEA fabrication process flow.

The 1, 2, and 3 h PDA samples with 500 nm SiO_2 deposited atop PDA were optically a purple-green coloration, indicative of previously established thin-film thickness-dependent color change properties of SiO_2.[64] As Figure 6A,B shows, in the visual light range (400−700 nm), the plain PC utilized presented 86% transmittance (N = 3). Optical clarity was observed to decrease in the 400−450 nm range with increased PDA deposition, as expected from the increased observed darkening of the PC. This decrease at 450 nm, for example, brought the overall transmittance to 75, 70, and 65%, respectively, at each timepoint (1, 2, and 3 h, respectively). Interestingly, corresponding PDA treatment times coupled with the 500 nm stable SiO_2 deposition demonstrated a moderate improvement of ∼3% transmittance on average, in addition to an antireflective signature shift. This reduction in transmittance is lessened greatly between 550 and 700 nm. This is of importance as many laser wavelengths utilized in excitation during fluorescence microscopy are found in this range. Unstable SiO_2 samples without PDA treatment were also tested and retain an irregular, antireflective-type signature (Figure 6A,B; red trace). These latter samples contained compressive strain-buckled SiO_2 mentioned previously and were poorly adherent.

An investigation into the characteristics of materials, and the potential stabilizing interactions between them was warranted. For stable film formation, there are several mechanisms through which bonding may be improved. Both the composition and increased surface roughness associated with the PDA-coating are more favorable than for the pristine PC, with the catechol-rich moieties present in the PDA providing strong bonding with a variety of other materials.[46,65] For confirmation of the layered composites, several material

https://doi.org/10.1021/acsami.3c05788
ACS Appl. Mater. Interfaces 2023, 15, 37157−37173

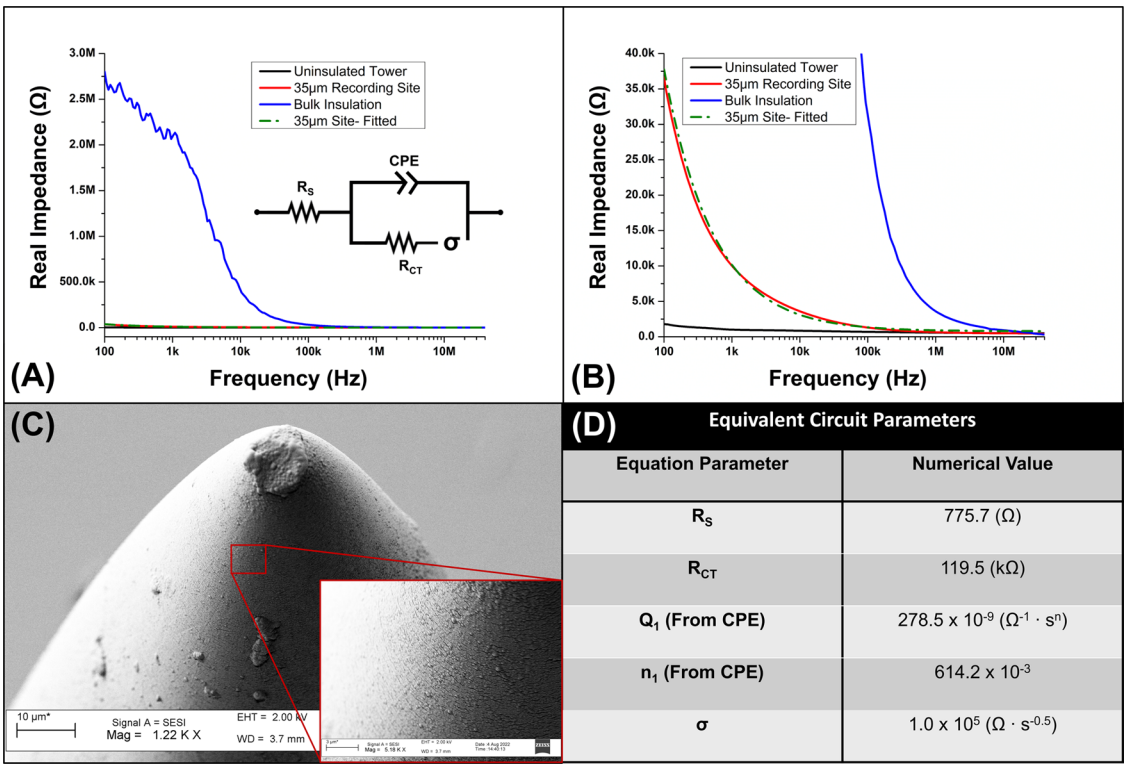

Equation Parameter	Numerical Value
R_S	775.7 (Ω)
R_{CT}	119.5 (kΩ)
Q_1 (From CPE)	278.5 x 10^{-9} ($Ω^{-1} \cdot s^n$)
n_1 (From CPE)	614.2 x 10^{-3}
σ	1.0 x 10^5 ($Ω \cdot s^{-0.5}$)

Figure 8. Microelectrode characterization of the fabricated 3D MEA, insulated with the optimized 2 h PDA−SiO_2 insulation strategy. (A) Full-spectrum impedance sweep of the defined microelectrodes at various states of insulation. As is apparent, the fully insulated microelectrode demonstrates a vastly greater impedance across much of the lower frequencies, as would be expected. The inset details the equivalent circuit utilized in fitting the final microelectrode. (B) Enhanced view of the data from panel (A), in which the uninsulated as well as the ∼35 μm microelectrode and associated fitting are better visualized. (C) SEM imaging of the full insulation on a SS microelectrode tower, provided by the 2 h PDA−SiO_2 insulation. The inset details a closer look at the conformal oxide-coating prior to precision laser deinsulation. (D) Extracted equivalent-circuit parameters from the final microelectrode fitting in panels (A, B).

analyses were performed. EDS analysis of the e-beam sublimated SiO_2 first confirmed the retention of the sublimated oxide composition (relative atomic percentages of 29.83% (Si) and 69.60% (O); see Figure S1B) as investigation continued. Next, HRTEM scans of PDA−SiO_2 on PC were performed (Figures 6C; S2). Through the cross section, three distinct layers were observed, confirming the presence of silicon (Si; blue), carbon (C; red), and oxygen (O; yellow). A clear interspersal of Si−O−C elements in the median layer was observed, which may be attributed to the bonding interactions of SiO_2 and PDA. Nitrogen (N; uncolored) is additionally present, as confirmed by the accompanying EDS scan (Figure S2); however; its relative abundance is overshadowed by larger quantities of the other elements. Its presence is additionally confirmed by XPS scans as reported later in this section.

PDA films strongly attenuate visible light,[66] evident with films only tens of nanometers in thickness.[67] As such, methodologies to generate uniform but thin coatings were employed (pH ∼ 8.0, 1−3 h of coating). To investigate the texture and wetting behavior of the PDA surface, water contact angle measurements and surface imaging techniques were performed (Figure 7A). A shift in the wetting behavior signals a shift in the surface composition or surface roughness. Pristine PC and SS surfaces exhibited minimal wetting, with contact angles of 78.5 ± 1.6 and 94.2 ± 4.6°, respectively. After several hours of PDA growth on these surfaces, a sharp drop in the wetting angle is observed, averaging 47.2 ± 1.2 and 43.6 ± 4.0° for PC and SS, respectively, across the 1−3 h times. The WCA values for each of the PDA treatment times is similar, with 2 h appearing the most consistent. The surface roughness of the PDA film would be distinct from the pristine surface and is thus indicative of the altered wetting behavior of surfaces. WCA values were also obtained for intermediary layers in the overall treatment regimen, serving to validate the assistance of mixed-air plasma treatments on adhesion, along with the strong hydrophilicity of sublimated SiO_2 films (Figure S3A).

Laser confocal microscopy was additionally performed to assess the relative increase in surface roughness after PDA and SiO_2 depositions, respectively (Figure S3B−D). The samples analyzed were PDA and SiO_2 on SS, as the optical properties of the film on PC presented measurement issues that prevented accurate results. Plain SS demonstrated an average surface roughness of 0.150 ± 0.036 μm, which was expected due to striations inherent in the machined steel sheet. After 2 h of PDA treatment, the surface roughness increased to 0.186 ± 0.036 μm, which represented a moderate increase, but as expected, did not differ greatly from the minor roughness of steel. After deposition of SiO_2, the surface roughness increased to 0.478 ± 0.140 μm, which was indicative of the presence of the bulk SiO_2 film, as had been observed under the SEM. Overall, we believe composition to be the main contributor to the wetting shift after WCA measurements and profilometry. This shift in surface energy of similarly fabricated PDA films was experimentally found to stabilize polymer film formation; however, the residual stresses of the SiO_2 film may not be solely stabilized by the interfacial energy, and surface interactions alone may not fully explain the improved integrity of the coating.

https://doi.org/10.1021/acsami.3c05788
ACS Appl. Mater. Interfaces 2023, 15, 37157−37173

We propose the PDA layer facilitated chemical bonding or intermixing between the SiO_2 at the interface. The wide variety of bonding modes and oxidation states available to PDA are shown in Figure 7B,C, with these bonds responsible for adhering a wide variety of inorganic and organic materials in the literature.[68] We found etching of thin films below thresholds where internal stress does not play a factor, where 10 nm is considered a nominally thin film. As such, ∼10 nm films (Figure S4) were deposited onto pristine PC and PDA-PC, and X-ray photoelectron spectroscopy (XPS) was utilized to investigate the nature of the bonding. Initial survey scans of plasma-treated PDA films demonstrated in significantly altered C 1s and N 1s binding energies and suggesting higher oxygen content binding sites (Figure S5). Further, XPS surveys of the 10 nm oxide films (Figure 7D) showed no significant difference between the two films. However, examining the higher-resolution scans demonstrate observed subtle shifts in Si 2p electrons. The spin−orbit splitting of the Si 2p electron is minor, typically on the scale of 0.63 eV and is not always deconvoluted in reports for silicon dioxide.[69] In these thinner films, which highlight the interface of SiO_2 attachment, there is another set of peaks detected in the SiO_2 peaks on the PDA layer, which suggests an altered Si environment near the PDA. In both signals, there is a typical $2p_{3/2}$ peak at 103.4 eV. When deposited on the PDA, a new set of peaks emerge with the $2p_{3/2}$ peak centered at 102.2 eV. We suspect that the localized thermal processes associated with the electron-beam deposition, along with the PDA structure and composition, play an important role in this interface formation. This shift may be associated with SiO_2 reacting in some capacity with the PDA, forming covalent bonds as represented in Figure 7E, or an intermixed diffusion layer through which strong adhesion may be promoted.

3.2. Impedimetric Performance of Fabricated 3D MEAs. Prior to their utilization as functional electrophysiological stimulation/recording devices, MEAs are regularly characterized for their electrical or impedimetric performance. Herein, the fabricated 3D MEAs were characterized at different stages of insulation definition to better visualize electrically (indirect measurement) the completion of the SiO_2-coating and definition (average $N = 4$ devices, Figure 8A,B). Prior to PDA−SiO_2-coating, the uninsulated microneedle towers demonstrated a 1 kHz impedance of 1.01 ± 3.24 kΩ, which would be suitable for electrophysiology in combination with a defined microelectrode recording site.[70,71] After insulation with PDA−SiO_2, the bulk insulated tower had a 1 kHz impedance of 2.0 ± 0.23 MΩ. This value was higher than desired for electrophysiological measurements but indicated a possibly distributed microelectrode surface spread across the length of the microtower structure. This hypothesis was confirmed by SEM imaging (Figure 8C), where nanoporous openings can be observed in the continuous SiO_2 film. This could explain the slightly enhanced noise in the functional electrophysiology presented in Section 3.3. After laser ablation, the final microelectrode was determined to be ∼35 μm^2 in size and presented a 1 kHz impedance of 10.2 ± 3.47 kΩ that is closer to other literature-reported MEA values.[28,48,72] The final ∼35 μm^2-sized 3D microelectrode was subsequently fitted with a modified Randles equivalent circuit to simulate and extract relevant parameters of interest (Figure 8A,D). Typically, a Randles circuit is comprised of the solution resistance (R_S), charge transfer resistance (R_{CT}), double layer capacitance (C_{DL}), and Warburg diffusion element (σ). As mentioned in Section 2.3.3, the C_{DL} component was replaced with a CPE, which flexibly acts as a capacitor while serving as a better-fitting element to experimental impedimetric recordings. Within 5% relative error, the model produced R_S of 775.7 Ω, R_{CT} of 119.5 kΩ, CPE Q of 278.5 × 10^{-9} ($\Omega^{-1} \cdot s^n$), n of 614.2 × 10^{-3}, and a Warburg diffusion σ value of 1.0 × 10^5 ($\Omega \cdot s^{-0.5}$).

3.3. Neural Organoid Growth and CAPs. Initially, rat-derived DRG spheroids were matured on transwells and transferred to SiO_2-insulated MEAs once there was substantial neurite outgrowth within their hydrogel scaffold. Previous iterations of this approach on earlier platforms[31,73] had shown robust growth of such constructs, but failed to yield functional recordings.[31] Figure S6A,B illustrates the comparative recording of rat-DRG CAPs following electrical stimulation of the distal nerve outgrowth at 5 weeks *in vitro* on earlier SiO_2-insulated platforms. While the MEA-recorded signal was able to detect some negative-going electrophysiological activity (mean amplitude maximum of −29 μV), a simultaneously recorded, more nuanced signal was present from the standard glass field electrode, with an amplitude maximum of −45 μV. Maximal recorded amplitudes may differ across recording modality and samples. However, comparable performance was observed as both recordings were of the same order of magnitude. These initial results indicated promise of the proposed 3D MEA microfabrication process for the intended MPS application, as the biological complexity and MEA development improved.

The human AHN-UWSCDH spheroidal constructs were cultured atop SiO_2-coated (Figure 2C,D) and glass control substrates in a defined dual-hydrogel format for 2 weeks and cultures were then stained with Calcein AM to assess viability (Figure 9A,B). Excellent neurite outgrowth was observed, lending credence to further utilize them within a neural MPS. Additional growth images are presented in the Supporting Information, further highlighting healthy cultures with robust

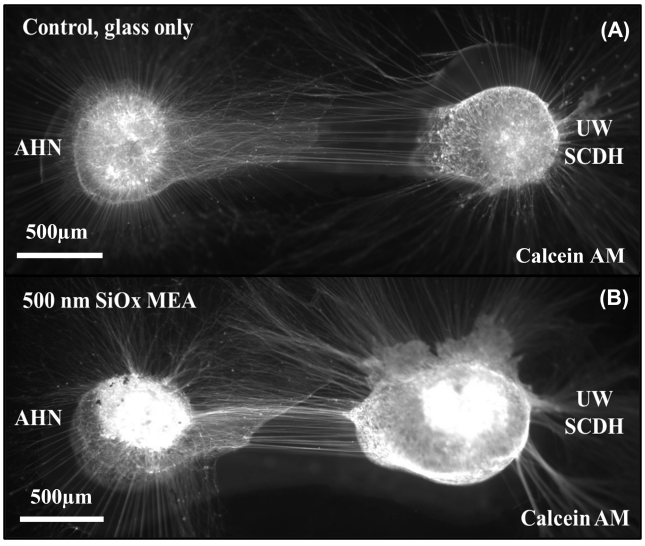

Figure 9. Fluorescence images of defined neural cocultures. (A) Fluorescence microscopy of the neural AHN-UWSCDH coculture on a control glass substrate demonstrating robust growth and viability. (B) Fluorescence imaging of coculture growth on the oxide-coated 3D MEA, illustrating comparable growth and excellent biocompatibility.

https://doi.org/10.1021/acsami.3c05788
ACS Appl. Mater. Interfaces 2023, 15, 37157−37173

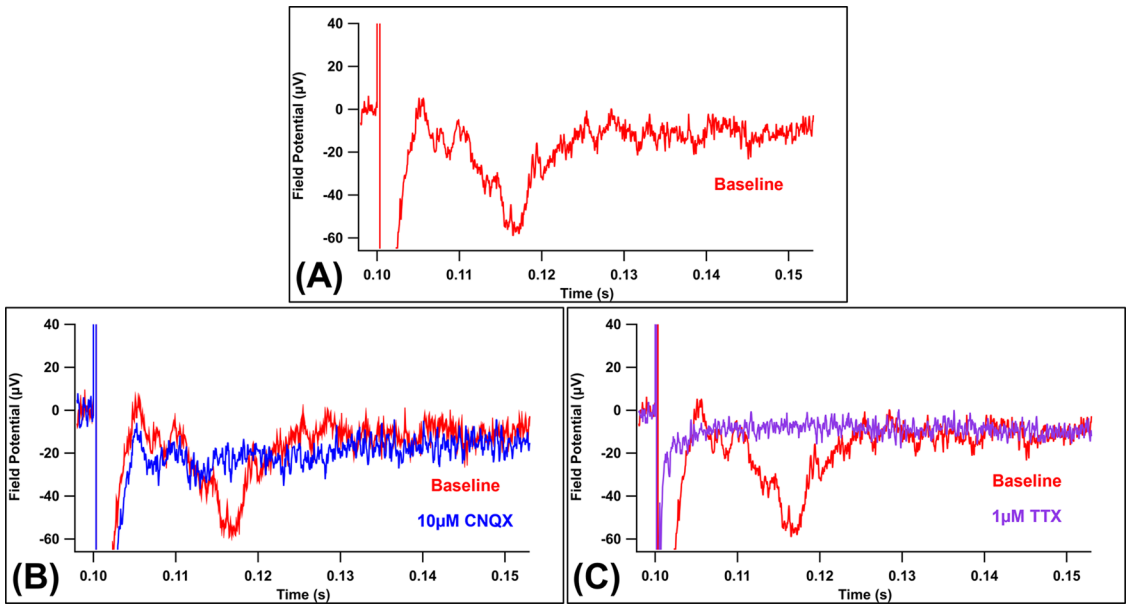

Figure 10. Electrophysiological recordings from a mature, 2 month human neural coculture on the 3D MEA. (A) Baseline electrophysiological signature from the coculture. (B) Addition of CNQX results in a partial loss of signaling; indicating the presence of glutamatergic synaptically-evoked field potentials. (C) Addition of TTX fully confirms the biological nature of the activity by blocking all signaling functions of the culture.

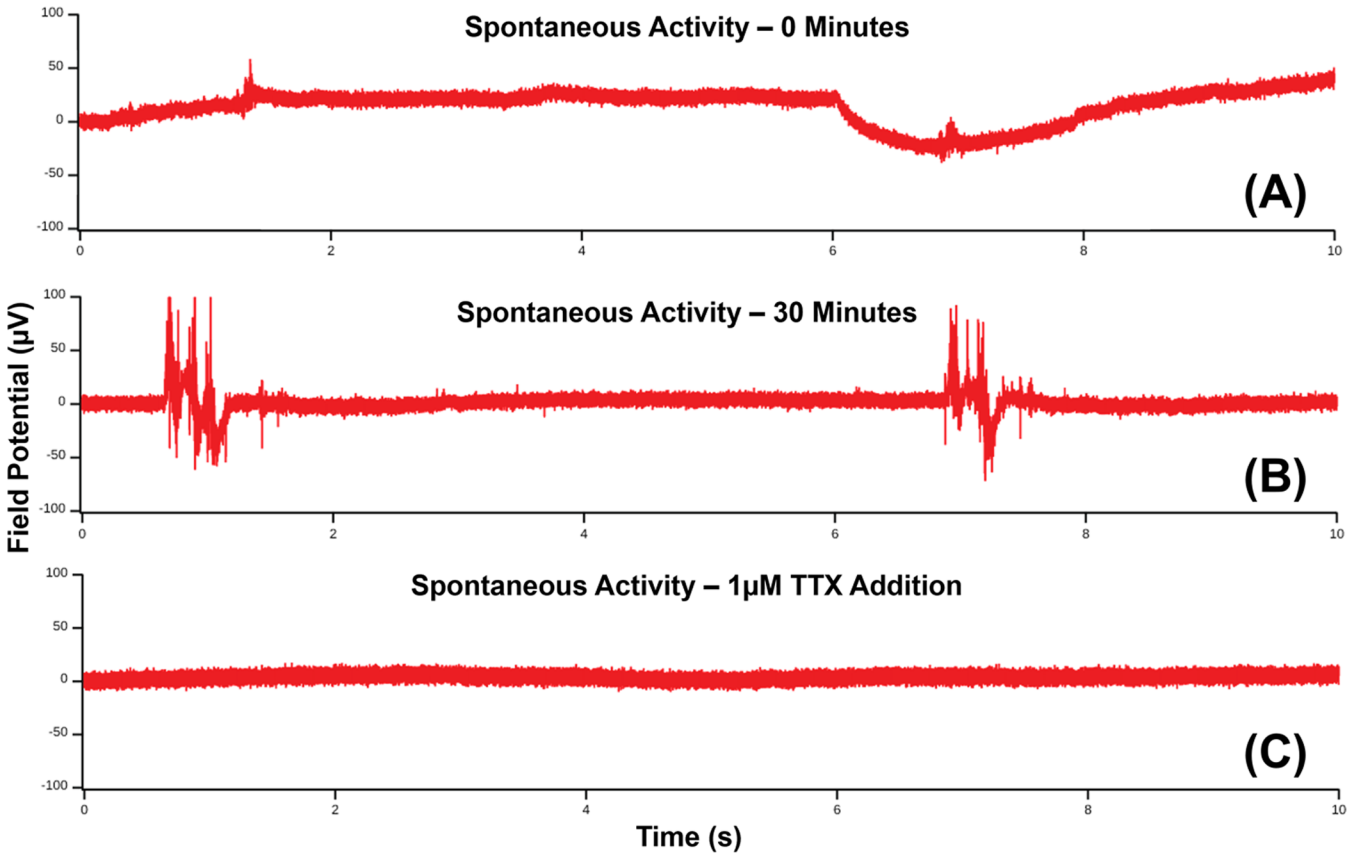

Figure 11. Spontaneous activity from a mature, 6 month human neural coculture on the 3D MEA. (A) Initial asynchronous activity after immediate immersion in artificial CSF. (B) Activity becomes more synchronous in nature after a 30 min acclimation period. (C) TTX is again added to remove all signaling and confirm the biological nature of the waveform.

neurite outgrowth on 3D MEAs (Figure S7). The synaptically evoked waveforms (i.e. CAPs) shown in Figure S6CD were recorded from a human AHN-UWSCDH construct, which was matured for 4 months on the 3D MEA. This recording derived from the integrated 3D MEA microelectrodes in this trial showcased two distinct negative-going peaks in the spinal cord spheroid (mean amplitude maximums of −10 and −5 μV, respectively). This again serves to demonstrate the suitability

https://doi.org/10.1021/acsami.3c05788
ACS Appl. Mater. Interfaces 2023, 15, 37157−37173

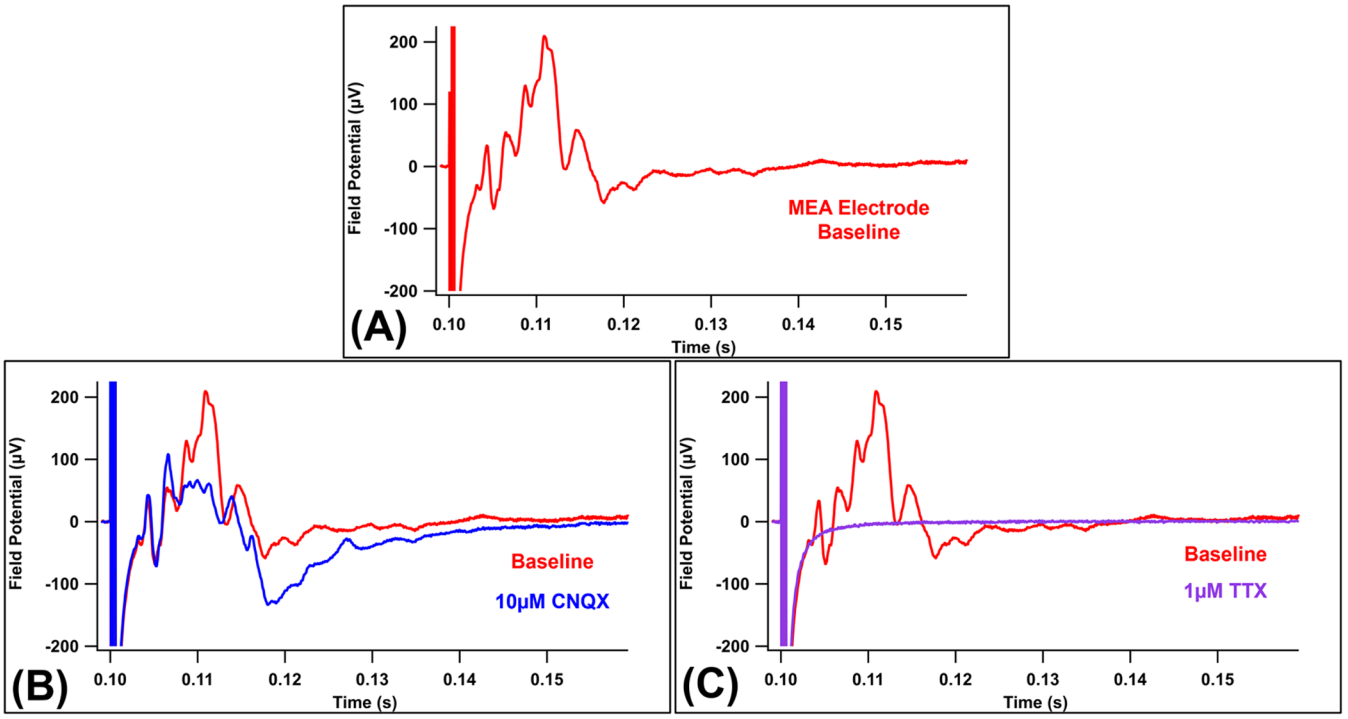

Figure 12. Electrophysiological response of the second mature, 6 month human neural coculture on a 3D MEA. (A) Baseline waveform of the coculture. Higher amplitudes and less noise are indicative of a well-integrated culture on the MEA. (B) CNQX was next added, and a partial loss of stimulated response was observed. (C) Finally, TTX was added, which abolished the waveform and again confirmed the true biological nature of the cocultured waveform.

of the 3D MEA for electrophysiological recordings, as well as highlight amplitude variations across cocultures.

More stable recordings with larger amplitudes were obtained from the complex human AHN-UWSCDH dual-spheroidal populations matured directly on 3D MEAs after final determination of the optimal PDA−SiO_2 treatment. As shown in Figure 10, internal 40 V stimulation of the afferent nociceptor spheroid (Figure 10A) elicited activity reminiscent of previously established synaptically evoked waveforms in the spinal cord spheroid of a construct matured for 2 months.[1] Two early negative-going peaks of −20 and −60 μV were detected within 20 ms of stimulation of the afferent nociceptor tissue and responded differently to application of the glutamatergic AMPA receptor inhibitor, CNQX. Application of 10 μM CNQX abolished the second −60 μV peak but not the first −20 μV peak, indicating that the second, but not first, peak resulted from glutamatergic synaptic activation (Figure 10B). The resulting secondarily recorded waveform retains some of the original CAP signature, demonstrating it to be distinct from general noise (Figure 10B). The earliest negative peak still appears present (−30 μV), while later activity has been predictably abolished. Finally, blockade of all voltage-gated sodium channel function through application of 1 μM TTX eliminated all detectable activity in the culture, confirming the biological nature of the entire waveform (Figure 10C).

AHN-UWSCDH cocultures remained viable for at least 6 months when cultured directly on the 3D MEA. Spontaneous waveform generation was also detectable at this timepoint (Figure 11), far exceeding the maximal postulated 10 week stability of SiO_2 insulation. When initially bathed in ACSF, one or two relatively small spontaneous bursts of activity occurred every 10 s (mean maximum amplitudes +70 μV/−45 μV; Figure 11A). After a 30 min equilibration time with no additional stimulation, spontaneous bursts became larger in amplitude but continued with a similar rate atop the 3D MEA (mean maximum amplitudes +100 μV/−75 μV; Figure 11B). Application of TTX abolished the production of spontaneous waveforms, again confirming that they are biological in nature (Figure 11C). Spontaneous burst firing has been described in similar neural microphysiological systems comprised of human stem-cell-derived neural tissue,[74] including spinal cord systems.[75] It was observed from these results that the specific coculture described appeared to undergo maturation between 2 and 6 months; only exhibiting spontaneous activity after exposure and equilibration to ACSF. Further experimentation will be necessary to characterize the underlying biological basis of the spontaneously produced waveforms described here.

The stimulation response of the 6 month matured, AHN-UWSCDH construct was then assessed utilizing the stimulation capabilities of the integrated 3D MEA. A 40 V pulse was applied to the afferent nociceptor spheroid once per minute through the internal 3D microelectrode and then was applied through a standard external field stimulating electrode manually inserted into the same nociceptor spheroid. The resulting synaptically evoked waveforms were recorded in the spinal cord spheroid through the integrated 3D MEA recording electrodes (trace average N = 10). The 3D MEA stimulating electrode evoked comparable baseline responses (mean maximal 3D MEA amplitudes +200 μV/−60 μV; Figure 12A) as compared to the external field electrode inserted into the same construct (Figure S6E). Such well-defined electrophysiological responses may potentially be attributed to the intimate integration of the MEA with the coculture over the 6 month growth period.

https://doi.org/10.1021/acsami.3c05788
ACS Appl. Mater. Interfaces 2023, 15, 37157−37173

Finally, synaptically evoked waveform production was assayed in the presence of CNQX and TTX to confirm the synaptic biological nature of these signatures. As shown in Figure 12B, application of 10 μM CNQX altered the shape of the synaptically evoked waveform beginning ~10 ms post-stimulation (mean amplitude maximums of +100 μV/−130 μV). As expected, application of 1 μM TTX again abolished all detectable field potentials, confirming their biological basis, (Figure 12C). Although these initial findings confirm the successful recording of a biological signal through this human stem-cell-derived neural circuit with integrated MEA stimulation and recording capabilities, further characterization is necessary to understand the entirety of the information provided by the electrophysiological signals.

4. CONCLUSIONS

In this work, we demonstrated a novel methodology for the hybridization of electron-beam sublimated silicon dioxide on polycarbonate and stainless steel 3D MEAs without the need for annealing. Due to the incompatibility of these materials with traditional SiO_2 deposition processes, a custom solution-based polydopamine intermediary was utilized. A 2 h PDA treatment, coupled with mixed-air plasma preparations, led to a stable 500 nm SiO_2 deposition on both materials. Following this combined treatment of PC, MEAs retained suitable transparency for imaging, due in part to the oxide layer.

Combinatorial characterizations were performed on the deposited silicon dioxide film, stabilized by polydopamine. Through SEM and laser confocal imaging, changes to surface roughness and surface topography were observed, lending support to the hypothesis that surface roughness plays a role in PDA interactions. WCA measurements were also obtained to demonstrate the effect of increasing surface energies on layered thin films. Finally, XPS analysis provides affirmative indications that through the utilization of PDA, Si−O bonds were formed, providing a combined interfacial energy and chemical bonding mechanism.

For functional 3D MEA application validation, SiO_2-coated SS demonstrated excellent adhesion retention for 6 weeks on test substrates and provided suitable dielectric performance from 6 month matured hPSC-derived, neural cultures. The ~35 μm^2 recording site defined on the 3D MEA presented a 1 kHz impedance of 10.2 kΩ, which proved to be stable for functional electrophysiological stimulation and recording. Early trials of MEAs presented smaller-amplitude waveforms from adult rat-derived primary DRG cultures but steadily improved to provide stimulation responses and repeatable recordings from 2 and 4 month matured human coculture constructs. These electrophysiological waveforms were confirmed to be distinctly biological in nature through inhibitory drug treatments (CNQX and TTX). Finally, 6 month matured human AHN-UWSCDH constructs on the 3D MEA demonstrated both spontaneous as well as synaptically evoked waveforms, which were again confirmed to be true biological signatures after blockade experiments through application of CNQX and TTX. Taken together, these results indicate the presence of a true complex biological waveform from the novel coculture described. While more experimentation and study are required to define the architecture of the overall waveform, the ability to resolve spontaneous, evoked, and drug-influenced activity indicates the suitability of this unique, custom, hybrid-material 3D MEA to be utilized in future neural MPS drug-sensitive screening applications specific to the proposed peripheral-spinal neural junction described in this work.

Overall, such microfabrication process flows allow for further development of practical and scalable BioMEMS devices that will enable invaluable advances in neural MPS circuits.

■ ASSOCIATED CONTENT

Supporting Information

The Supporting Information is available free of charge at https://pubs.acs.org/doi/10.1021/acsami.3c05788.

Data for additional peel tests, HRTEM EDS, WCA measurements, laser confocal, SEM images, XPS spectra, compound action potentials, and coculture images (PDF)

■ AUTHOR INFORMATION

Corresponding Author

Swaminathan Rajaraman − *University of Central Florida, Orlando, Florida 32816, United States; Primordia Biosystems Inc., Orlando, Florida 32804, United States*; Email: Swaminathan.Rajaraman@ucf.edu

Authors

Charles M. Didier − *University of Central Florida, Orlando, Florida 32816, United States*; orcid.org/0000-0002-5556-8694

David Fox − *University of Central Florida, Orlando, Florida 32816, United States*

Kevin J. Pollard − *Tulane University, New Orleans, Louisiana 70118, United States*

Aliyah Baksh − *University of Central Florida, Orlando, Florida 32816, United States*

Nisha R. Iyer − *University of Wisconsin-Madison, Madison, Wisconsin 53717, United States*

Alexander Bosak − *Tulane University, New Orleans, Louisiana 70118, United States*

Yuen Yee Li Sip − *University of Central Florida, Orlando, Florida 32816, United States*

Julia F. Orrico − *University of Central Florida, Orlando, Florida 32816, United States*

Avra Kundu − *University of Central Florida, Orlando, Florida 32816, United States*

Randolph S. Ashton − *University of Wisconsin-Madison, Madison, Wisconsin 53717, United States*

Lei Zhai − *University of Central Florida, Orlando, Florida 32816, United States*; orcid.org/0000-0002-3886-2154

Michael J. Moore − *Tulane University, New Orleans, Louisiana 70118, United States; AxoSim Inc., New Orleans, Louisiana 70112, United States*

Complete contact information is available at: https://pubs.acs.org/10.1021/acsami.3c05788

Author Contributions

#C.M.D., D.F., and K.J.P. contributed equally to this work through experimentation, writing, and assembly of the manuscript.

Notes

The authors declare the following competing financial interest(s): The authors would like to declare conflicts of interest relating solely to the potential for future licensing of some of the technologies described in this article for commercialization. The persons/entities of note include:

Professor S. Rajaraman (co-founder of Primordia BioSystems Inc.), and Professor M.J. Moore (co-founder AxoSim Inc.).

■ ACKNOWLEDGMENTS

The authors acknowledge the funding provided through the NIH NCATS HEAL Initiative, in the form of NIH UG3TR003150 and NIH UH3TR003150 grants, as well as through the UCF ORC Doctoral Fellowship (C.M.D.). The authors also acknowledge the NSTC, MCF-AMPAC, MSE, and ECE facilities at UCF for tool usage. The authors additionally acknowledge Kailyn M. Mariot for providing additional schematic renderings for this work as well as Guntis Rutins for his assistance with AFM profilometry measurements.

■ REFERENCES

(1) Pollard, K. J.; Bowser, D. A.; Anderson, W. A.; Meselhe, M.; Moore, M. J. Morphine-Sensitive Synaptic Transmission Emerges In Embryonic Rat Microphysiological Model Of Lower Afferent Nociceptive Signaling. *Sci. Adv.* **2021**, *7*, No. eabj2899.

(2) Anderson, W. A.; Bosak, A.; Hogberg, H. T.; Hartung, T.; Moore, M. J. Advances In 3D Neuronal Microphysiological Systems: Towards A Functional Nervous System On A Chip. *In Vitro Cell. Dev. Biol.: Anim.* **2021**, *57*, 191−206.

(3) Wikswo, J. P. The Relevance And Potential Roles Of Microphysiological Systems In Biology And Medicine. *Exp. Biol. Med.* **2014**, *239*, 1061−1072.

(4) Kang, S.-M. Recent Advances in Microfluidic-Based Microphysiological Systems. *BioChip J.* **2022**, *16*, 13−26.

(5) Pamies, D.; Barrera, P.; Block, K.; Makri, G.; Kumar, A.; Wiersma, D.; Smirnova, L.; Zhang, C.; Bressler, J.; Christian, K. M.; Harris, G. A. A Human Brain Microphysiological System Derived From Induced Pluripotent Stem Cells To Study Neurological Diseases And Toxicity. *ALTEX* **2017**, *34*, 362−376.

(6) Haring, A. P.; Sontheimer, H.; Johnson, B. N. Microphysiological Human Brain and Neural Systems-on-a-Chip: Potential Alternatives to Small Animal Models and Emerging Platforms for Drug Discovery and Personalized Medicine. *Stem Cell Rev. Rep.* **2017**, *13*, 381−406.

(7) Kratz, S.; Höll, G.; Schuller, P.; Ertl, P.; Rothbauer, M. Latest Trends In Biosensing For Microphysiological Organs-On-A-Chip And Body-On-A-Chip Systems. *Biosensors* **2019**, *9*, 110.

(8) Cai, H.; Ao, Z.; Tian, C.; Wu, Z.; Kaurich, C.; Chen, Z.; Gu, M.; Hohmann, A. G.; Mackie, K.; Guo, F. Engineering Human Spinal Microphysiological Systems To Model Opioid-Induced Tolerance. *Bioactive Mater.* **2023**, *22*, 482−490.

(9) Wang, Y. I.; Carmona, C.; Hickman, J. J.; Shuler, M. L. Multiorgan Microphysiological Systems For Drug Development: Strategies, Advances, And Challenges. *Adv. Healthcare Mater.* **2018**, *7*, No. 1701000.

(10) Nichols, K.; Koppes, R.; Koppes, A. Recent Advancements In Microphysiological Systems For Neural Development And Disease. *Curr. Opin. Biomed. Eng.* **2020**, *14*, 42−51.

(11) Molina-Martínez, B.; Jentsch, L. V.; Ersoy, F.; van der Moolen, M.; Donato, S.; Ness, T. V.; Heutink, P.; Jones, P. D.; Cesare, P. A. A Multimodal 3D Neuro-Microphysiological System With Neurite-Trapping Microelectrodes. *Biofabrication* **2022**, *14*, No. 025004.

(12) Dowden, H.; Munro, J. Trends In Clinical Success Rates And Therapeutic Focus. *Nat. Rev. Drug Discovery* **2019**, *18*, 495−496.

(13) Hargrove-Grimes, P.; Low, L. A.; Tagle, D. A. Microphysiological Systems: What It Takes For Community Adoption. *Exp. Biol. Med.* **2021**, *246*, 1435−1446.

(14) Volkow, N. D.; Collins, F. S. The Role Of Science In Addressing The Opioid Crisis. *N. Engl. J. Med.* **2017**, *377*, 391−394.

(15) Didier, C. M.; Fox, D.; Baksh, A.; Pollard, K.; Iyer, N.; Bosak, A.; Orrico, J.; Castro, J. M.; Kundu, A.; Zhai, L.; Ashton, R. S.; Moore, M. J.; Rajaraman, S. Stable, Electron-Beam Sublimated, Nanostructured Silicon Dioxide On Polycarbonate And Stainless-Steel As A Bioadherent Dielectric Towards Neural Microphysiological Systems. In *Hilton Head 2022 MEMS Workshop* Hilton Head, SC;2022.

(16) Bai, X.; Wang, K.; Chen, L.; Zhou, J.; Wang, J. Semiconducting Polymer Dots As Fluorescent Probes For In Vitro Biosensing. *J. Mater. Chem. B* **2022**, *10*, 6248−6262.

(17) Zhang, S.; Rong, F.; Guo, C.; Duan, F.; He, L.; Wang, M.; Zhang, Z.; Kang, M.; Du, M. Metal−Organic Frameworks (Mofs) Based Electrochemical Biosensors For Early Cancer Diagnosis In Vitro. *Coord. Chem. Rev.* **2021**, *439*, No. 213948.

(18) Janegitz, B. C.; Silva, T. A.; Wong, A.; Ribovski, L.; Vicentini, F. C.; Sotomayor, M. D.; Fatibello-Filho, O. The Application Of Graphene For In Vitro And In Vivo Electrochemical Biosensing. *Biosens. Bioelectron.* **2017**, *89*, 224−233.

(19) Didier, C. M.; Kundu, A.; Shoemaker, J. T.; Vukasinovic, J.; Rajaraman, S. SeedEZ Interdigitated Electrodes and Multifunctional Layered Biosensor Composites (MLBCs): A Paradigm Shift in the Development of In Vitro BioMicrosystems. *J. Microelectromech. Syst.* **2020**, *29*, 653−660.

(20) Kim, J.; Koo, B-K.; Knoblich, J. A. Human Organoids: Model Systems For Human Biology And Medicine. *Nat. Rev. Mol. Cell Biol.* **2020**, *21*, 571−584.

(21) Didier, C. M.; Kundu, A.; Deroo, D.; Rajarman, S. Development of In Vitro 2D and 3D Microelectrode Arrays and Their Role in Advancing Biomedical Research. *J. Micromech. Microeng.* **2020**, *30*, 103001.

(22) Choi, J. S.; Lee, H. J.; Rajaraman, S.; Kim, D-H. Recent Advances In Three-Dimensional Microelectrode Array Technologies For In Vitro And In Vivo Cardiac And Neuronal Interfaces. *Biosens. Bioelectron.* **2021**, *171*, No. 112687.

(23) Park, Y.; Franz, C. K.; Ryu, H.; Luan, H.; Cotton, K. Y.; Kim, J. U.; Chung, T. S.; Zhao, S.; Vazquez-Guardado, A.; Yang, D. S.; Li, K.; et al. Three-Dimensional, Multifunctional Neural Interfaces For Cortical Spheroids And Engineered Assembloids. *Sci. Adv.* **2021**, *7*, No. eabf9153.

(24) Kalmykov, A.; Huang, C.; Bliley, J.; Shiwarski, D.; Tashman, J.; Abdullah, A.; Rastogi, S. K.; Shukla, S.; Mataev, E.; Feinberg, A. W.; Hsia, K. J.; Cohen-Karni, T. Organ-On-E-Chip: Three-Dimensional Self-Rolled Biosensor Array For Electrical Interrogations Of Human Electrogenic Spheroids. *Sci. Adv.* **2019**, *5*, No. eaax0729.

(25) Xu, S.; Deng, Y.; Luo, J.; He, E.; Liu, Y.; Zhang, K.; Yang, Y.; Xu, S.; Sha, L.; Song, Y.; Xu, Q.; Cai, X. High-Throughput PEDOT:PSS/PtNPs-Modified Microelectrode Array for Simultaneous Recording and Stimulation of Hippocampal Neuronal Networks in Gradual Learning Process. *ACS Appl. Mater. Interfaces* **2022**, *14*, 15736−15746.

(26) Tomaskovic-Crook, E.; Tomaskovic-Crook, E.; Zhang, P.; Ahtiainen, A.; Kaisvuo, H.; Lee, C. Y.; Beirne, S.; Aqrawe, Z.; Svirskis, D.; Hyttinen, J.; Wallace, G. G.; Travas-Sejdic, J.; Travas-Sejdic, J. Human Neural Tissues From Neural Stem Cells Using Conductive Biogel And Printed Polymer Microelectrode Arrays For 3D Electrical Stimulation. *Adv. Healthcare Mater.* **2019**, *8*, No. 1900425.

(27) Didier, C. M.; Kundu, A.; Rajaraman, S. Rapid Makerspace Microfabrication and Characterization of 3D Microelectrode Arrays (3D MEAs) for Organ-on-a-Chip Models. *J. Microelectromech. Syst.* **2021**, *30*, 853−863.

(28) Kundu, A.; McCoy, L.; Azim, N.; Nguyen, H.; Didier, C. M.; Ausaf, T.; Sharma, A. D.; Curley, J. L.; Moore, M. J.; Rajaraman, S. Fabrication and Characterization of 3D Printed, 3D Microelectrode Arrays for Interfacing with a Peripheral Nerve-on-a-Chip. *ACS Biomater. Sci. Eng.* **2021**, *7*, 3018−3029.

(29) Jin, X.; Strueben, J.; Heepe, L.; Kovalev, A.; Mishra, Y. K.; Adelung, R.; Gorb, S. N.; Staubitz, A. Joining the Un-Joinable: Adhesion Between Low Surface Energy Polymers Using Tetrapodal ZnO Linkers. *Adv. Mater.* **2012**, *24*, 5676−5680.

(30) Kramer, L.; Nguyen, H. T.; Jacobs, E.; McCoy, L.; Curley, J. L.; Sharma, A. D.; Moore, M. J. Modeling Chemotherapy-Induced

Peripheral Neuropathy Using A Nerve-On-A-Chip Microphysiological System. *ALTEX* **2020**, *37*, 350−364.
(31) Didier, C. M.; Rountree, C.; Orrico, J. F.; Kundu, A.; Azim, N.; Nguyen, H.; Pasha, S. K.; McCoy, L.; Curley, J. L.; Moore, M. J.; Rajaraman, S. Fabrication and Characterization of 3D Microelectrode Arrays (3D MEAs) with "Edge-Wrapped" Metal Interconnects and 3D-Printed Assembly Rigs for Simultaneous Optical and Electrical Probing of Nerve-on-a-Chip Constructs. In *2021 IEEE 34th International Conference on Micro Electro Mechanical Systems (MEMS)* 2021; pp 226−229.
(32) Kim, G. H.; Kim, K.; Lee, E.; An, T.; Choi, W.; Lim, G.; Shin, J. H. Recent Progress on Microelectrodes in Neural Interfaces. *Materials* **2018**, *11*, 1995.
(33) Lee, H.; Shin, K.; Moon, W. Capacitive Measurements of SiO_2 Films of Different Thicknesses Using a MOSFET-Based SPM Probe. *Sensors* **2021**, *21*, 4073.
(34) Coln, E. A.; Colon, A.; Long, C. J.; Sriram, N. N.; Esch, M.; Prot, J. M.; Elbrecht, D. H.; Wang, Y.; Jackson, M.; Shuler, M. L.; Hickman, J. J. Piezoelectric BioMEMS Cantilever For Measurement Of Muscle Contraction And For Actuation Of Mechanosensitive Cells. *MRS Commun.* **2019**, *9*, 1186−1192.
(35) Susloparova, A.; Halliez, S.; Begard, S.; Colin, M.; Buée, L.; Pecqueur, S.; Alibart, F.; Thomy, V.; Arscott, S.; Pallecchi, E.; Coffinier, Y. Low Impedance And Highly Transparent Microelectrode Arrays (MEA) For In Vitro Neuron Electrical Activity Probing. *Sens. Actuators, B* **2021**, *327*, No. 128895.
(36) Middya, S.; Curto, V. F.; Fernández-Villegas, A.; Robbins, M.; Gurke, J.; Moonen, E. J.; Kaminski Schierle, G. S.; Malliaras, G. G. Microelectrode Arrays for Simultaneous Electrophysiology and Advanced Optical Microscopy. *Adv. Sci.* **2021**, *8*, No. 2004434.
(37) Sessolo, M.; Khodagholy, D.; Rivnay, J.; Maddalena, F.; Gleyzes, M.; Steidl, E.; Buisson, B.; Malliaras, G. G. Easy-to-Fabricate Conducting Polymer Microelectrode Arrays. *Adv. Mater.* **2013**, *25*, 2135−2139.
(38) Delivopoulos, E.; Ouberai, M. M.; Coffey, P. D.; Swann, M. J.; Shakesheff, K. M.; Welland, M. E. Serum Protein Layers On Parylene-C And Silicon Oxide: Effect On Cell Adhesion. *Colloids Surf., B* **2015**, *126*, 169−177.
(39) Unsworth, C. P.; Holloway, H.; Delivopoulos, E.; Murray, A. F.; Simpson, M. C.; Dickinson, M. E.; Graham, E. S. Patterning And Detailed Study Of Human HNT Astrocytes On Parylene-C/Silicon Dioxide Substrates To The Single Cell Level. *Biomaterials* **2011**, *32*, 6541−6550.
(40) Unsworth, C. P.; Delivopoulos, E.; Gillespie, T.; Murray, A. F. Isolating Single Primary Rat Hippocampal Neurons & Astrocytes On Ultra-Thin Patterned Parylene-C/Silicon Dioxide Substrates. *Biomaterials* **2011**, *32*, 2566−2574.
(41) Allahyari, Z.; Gaborski, T. R. Engineering Cell−Substrate Interactions On Porous Membranes For Microphysiological Systems. *Lab Chip* **2022**, *22*, 2080−2089.
(42) Amirzada, M. R.; Tatzel, A.; Viereck, V.; Hillmer, H. Surface Roughness Analysis Of SiO_2 For PECVD, PVD And IBD On Different Substrates. *Appl. Nanosci.* **2016**, *6*, 215−222.
(43) Omnexus. Glass Transition Temperature. In Omnexus Special Chemistry; 2022 https://omnexus.specialchem.com/polymer-properties/properties/glass-transition-temperature.
(44) Kushner, D. I.; Hickner, M. A. Water Sorption in Electron-Beam Evaporated SiO_2 on QCM Crystals and Its Influence on Polymer Thin Film Hydration Measurements. *Langmuir* **2017**, *33*, 5261−5268.
(45) Azim, N.; Orrico, J. F.; Gupta, D. A.; Zhai, L.; Rajaraman, S. Polydopamine Surface Functionalization Of 3D Printed Resin Material For Enhanced Polystyrene Adhesion Towards Insulation Layers For 3D Microelectrode Arrays (3D MEAs). *RSC Adv.* **2022**, *12*, 25605−25616.
(46) Lee, H.; Dellatore, S. M.; Miller, W. M.; Messersmith, P. B. Mussel-Inspired Surface Chemistry for Multifunctional Coatings. *Science* **2007**, *318*, 426−430.
(47) Kang, K.; Choi, I. S.; Nam, Y. A Biofunctionalization Scheme For Neural Interfaces Using Polydopamine Polymer. *Biomaterials* **2011**, *32*, 6374−6380.
(48) Orrico, J. F.; Kundu, A.; Didier, C. M.; Bosak, A.; Moore, M. J.; Rajaraman, S. Fabrication and Characterization of 3D Microelectrode Arrays (3D MEAS) with Tri-Modal (Electrical, Optical, and Microfluidic) Interrogation of Electrogenic Cell Constructs. In *2021 21st International Conference on Solid-State Sensors, Actuators and Microsystems (Transducers)*, 2021; pp 767−770.
(49) Rezaee, M.; Tsai, L-C.; Haider, M. I.; Yazdi, A.; Sanatizadeh, E.; Salowitz, N. P. Quantitative Peel Test For Thin Films/Layers Based On A Coupled Parametric And Statistical Study. *Sci. Rep.* **2019**, *9*, No. 19805.
(50) Ragoisha, G. A.; Bondarenko, A. S. Potentiodynamic Electrochemical Impedance Spectroscopy. *Electrochim. Acta* **2005**, *50*, 1553−1563.
(51) Bondarenko, A. S.; Ragoisha, G. A. EIS Spectrum Analyser - Equivalent Circuit Elements and Parameters, 2008.
(52) Didier, C. M.; Orrico, J. F.; Cepeda-Torres, O. S.; Castro, J. M.; Baksh, A.; Rajaraman, S. Microfabricated Polymer-Metal Biosensors For Multifarious Data Collection From Electrogenic Cellular Models. *Microsyst. Nanoeng.* **2022**, *9*, 22.
(53) Castro, J. M.; Rajaraman, S. Constant Phase Element (CPE) Modeling And Analysis Of Multi-Material, Micro-Bullet Shaped, High-Throughput 3D Microelectrodes For In-VIitro Electrophysiological Applications. In *Proceedings of the 2022 Hilton Head MEMS Workshop 2022*.
(54) Bowser, D. A.; Moore, M. J. Biofabrication Of Neural Microphysiological Systems Using Magnetic Spheroid Bioprinting. *Biofabrication* **2020**, *12*, No. 015002.
(55) Curley, J. L.; Moore, M. J. Facile Micropatterning Of Dual Hydrogel Systems For 3D Models Of Neurite Outgrowth. *J. Biomed. Mater. Res. A* **2011**, *99A*, 532−543.
(56) Huval, R. M.; Miller, O. H.; Curley, J. L.; Fan, Y.; Hall, B. J.; Moore, M. J. Microengineered Peripheral Nerve-On-A-Chip For Preclinical Physiological Testing. *Lab Chip* **2015**, *15*, 2221−2232.
(57) Khoshakhlagh, P.; Sivakumar, A.; Pace, L. A.; Sazer, D. W.; Moore, M. J. Methods For Fabrication And Evaluation Of A 3D Microengineered Model Of Myelinated Peripheral Nerve. *J. Neural Eng.* **2018**, *15*, No. 064001.
(58) Sharma, A. D.; McCoy, L.; Jacobs, E.; Willey, H.; Behn, J. Q.; Nguyen, H.; Bolon, B.; Curley, J. L.; Moore, M. J. Engineering A 3D Functional Human Peripheral Nerve In Vitro Using The Nerve-On-A-Chip Platform. *Sci. Rep.* **2019**, *9*, No. 8921.
(59) Iyer, N. R.; Shin, J.; Cuskey, S.; Tian, Y.; Nicol, N. R.; Doersch, T. E.; Seipel, F.; McCalla, S. G.; Roy, S.; Ashton, R. S. Modular Derivation Of Diverse, Regionally Discrete Human Posterior CNS Neurons Enables Discovery Of Transcriptomic Patterns. *Sci. Adv.* **2021**, *8*, No. eabn7430.
(60) Sarangan, A. Quantum Mechanics And Computation In Nanophotonics. In *Fundamentals and Applications of Nanophotonics*; Woodhead Publishing, 2016; pp 45−87.
(61) Jubault, M.; Pulpytel, J.; Cachet, H.; Boufendi, L.; Arefi-Khonsari, F. Deposition Of SNo2: F Thin Films On Polycarbonate Substrates By PECVD For Antifouling Properties. *Plasma Process. Polym.* **2007**, *4*, S330−S335.
(62) Moon, M. W.; Chung, J. W.; Lee, K. R.; Oh, K. H.; Wang, R.; Evans, A. G. An Experimental Study Of The Influence Of Imperfections On The Buckling Of Compressed Thin Films. *Acta Mater.* **2002**, *50*, 1219−1227.
(63) Coupeau, C. Atomic Force Microscopy Study Of The Morphological Shape Of Thin Film Buckling. *Thin Solid Films* **2002**, *406*, 190−194.
(64) Henrie, J.; Kellis, S.; Schultz, S. M.; Hawkins, A. Electronic Color Charts For Dielectric Films On Silicon. *Opt. Express* **2004**, *12*, 1464−1469.
(65) Ding, Y. H.; Floren, M.; Tan, W. Mussel-Inspired Polydopamine For Bio-Surface Functionalization. *Biosurf. Biotribol.* **2016**, *2*, 121−136.

(66) Zou, Y.; Chen, X.; Yang, P.; Liang, G.; Yang, Y.; Gu, Z.; Li, Y. Regulating The Absorption Spectrum Of Polydopamine. *Sci. Adv.* **2020**, *6*, No. eabb4696.
(67) Hong, S.; Wang, Y.; Park, S. Y.; Lee, H. Progressive Fuzzy Cation-Π; Assembly Of Biological Catecholamines. *Sci. Adv.* **2018**, *4*, No. eaat7457.
(68) Xie, X.; Tang, J.; Xing, Y.; Wang, Z.; Ding, T.; Zhang, J.; Cai, K. Intervention of Polydopamine Assembly and Adhesion on Nanoscale Interfaces: State-of-the-Art Designs and Biomedical Applications. *Adv. Healthcare Mater.* **2021**, *10*, No. 2002138.
(69) Major, G. H.; Fairley, N.; Sherwood, P.; Linford, M. R.; Terry, J.; Fernandez, V.; Artyushkova, K. Practical Guide For Curve Fitting In X-Ray Photoelectron Spectroscopy. *J. Vacuum Sci. Technol. A* **2020**, *38*, No. 061203.
(70) Franks, W.; Schenker, I.; Schmutz, P.; Hierlemann, A. Impedance Characterization And Modeling Of Electrodes For Biomedical Applications. *IEEE Trans. Biomed. Eng.* **2005**, *52*, 1295−1302.
(71) Borkholder, D. *Cell Based Biosensors Using Microelectrodes*; Stanford University, 1998.
(72) Rajaraman, S. *Micromachined Three-Dimensional Electrode Arrays For In-Vitro And In-Vivo Electrogenic Cellular Networks*; Georgia Institute of Technology, 2009.
(73) Didier, C. M.; Kundu, A.; Rajaraman, S.Facile, Packaging Substrate-Agnostic, Microfabrication and Assembly of Scalable 3D Metal Microelectrode Arrays for in Vitro Organ-on-a-Chip and Cellular Disease Modeling. In *20th International Conference on Solid-State Sensors, Actuators and Microsystems & Eurosensors XXXIII (TRANSDUCERS & EUROSENSORS XXXIII)* 2019; pp 1686−1689.
(74) Woodruff, G.; Phillips, N.; Carromeu, C.; Guicherit, O.; White, A.; Johnson, M.; Zanella, F.; Anson, B.; Lovenberg, T.; Bonaventure, P.; Harrington, A. W. Screening For Modulators Of Neural Network Activity In 3d Human Ipsc-Derived Cortical Spheroids. *PLoS One* **2020**, *15*, No. e0240991.
(75) Lee, J. H.; Shin, H.; Shaker, M. R.; Kim, H. J.; Park, S. H.; Kim, J. H.; Lee, N.; Kang, M.; Cho, S.; Kwak, T. H.; Kim, J. W.; et al. Production Of Human Spinal-Cord Organoids Recapitulating Neural-Tube Morphogenesis. *Nat. Biomed. Eng.* **2022**, *6*, 435−448.

https://doi.org/10.1021/acsami.3c05788
ACS Appl. Mater. Interfaces 2023, 15, 37157−37173